Global Biogeochemical Cycles®

RESEARCH ARTICLE
10.1029/2021GB007072

Phytoplankton-Nitrifier Interactions Control the Geographic Distribution of Nitrite in the Upper Ocean

Xianhui S. Wan[1,2], Hua-Xia Sheng[3], Minhan Dai[1,3], Matthew J. Church[4], Wenbin Zou[1], Xiaolin Li[1,3], David A. Hutchins[5], Bess B. Ward[6], and Shuh-Ji Kao[1,3]

[1]State Key Laboratory of Marine Environmental Sciences, Xiamen University, Xiamen, China, [2]Now at Department of Geosciences, Princeton University, Princeton, NJ, USA, [3]College of Ocean and Earth Science, Xiamen University, Xiamen, China, [4]Flathead Lake Biological Station, University of Montana, Polson, MT, USA, [5]Department of Biological Sciences, University of Southern California, Los Angeles, CA, USA, [6]Department of Geosciences, Princeton University, Princeton, NJ, USA

Xianhui S. Wan and Hua-Xia Sheng contributed equally to this work.

Key Points:

- At the basin scale, the PNM exhibits a unique meridional pattern
- Nitrate-dependent phytoplankton-nitrifier interactions result in distinctive nitrite accumulation patterns in different ocean regions
- Following ammonia oxidation, urea oxidation represents the second largest nitrite source playing an essential role to form the PNM

Supporting Information:

Supporting Information may be found in the online version of this article.

Correspondence to:

S.-J. Kao,
sjkao@xmu.edu.cn

Citation:

Wan, X. S., Sheng, H.-X., Dai, M., Church, M. J., Zou, W., Li, X., et al. (2021). Phytoplankton-nitrifier interactions control the geographic distribution of nitrite in the upper ocean. *Global Biogeochemical Cycles*, *35*, e2021GB007072. https://doi.org/10.1029/2021GB007072

Received 14 MAY 2021
Accepted 7 OCT 2021

Author Contributions:

Conceptualization: Xianhui S. Wan, Hua-Xia Sheng
Data curation: Hua-Xia Sheng
Formal analysis: Xianhui S. Wan, Matthew J. Church, David A. Hutchins, Bess B. Ward
Funding acquisition: Hua-Xia Sheng, Minhan Dai, Matthew J. Church
Investigation: Xianhui S. Wan, Hua-Xia Sheng, Minhan Dai, Wenbin Zou, Xiaolin Li
Methodology: Xianhui S. Wan, Hua-Xia Sheng
Resources: Minhan Dai
Validation: Xianhui S. Wan, Hua-Xia Sheng, Matthew J. Church, Bess B. Ward

Abstract As a key intermediate in the nitrogen cycle, nitrite is involved in multiple biological pathways that regulate the distribution and availability of nitrogen in the ocean. In the oligotrophic gyres, nitrite accumulates near the base of the euphotic zone, demonstrating a subsurface maximum, termed the primary nitrite maximum; while in subpolar regions, nitrite concentrations are elevated in the near-surface ocean. As yet, the mechanisms controlling this meridional pattern remain unclear. Here, we present vertically resolved profiles of rates of nitrite production and consumption extending from the Subtropical Gyre to the Subarctic Front in the North Pacific Ocean. Our results indicate that the latitudinal distributions of nitrite across this basin are influenced by variations in phytoplankton-nitrifier interactions. In the well-lit oligotrophic surface, phytoplankton dominates rapid nitrite cycling via coupled release and re-assimilation; below the euphotic zone, diminished light stress on nitrite oxidizers results in rapid turnover and limits nitrite. By contrast, in subpolar regions where nitrate concentrations are elevated in the euphotic zone, nitrite is released during assimilative nitrate reduction and competition between phytoplankton and nitrifiers for ammonium is relaxed, facilitating ammonia oxidation. These processes, together with differential light sensitivities of ammonia and nitrite oxidizers, allow net accumulation of nitrite. Furthermore, we demonstrate a substantial contribution of urea oxidation in forming the primary nitrite maximum and balancing the two steps of marine nitrification. Our findings reveal physical-biological interactive controls on nitrite cycling and distributions in the ocean and help disentangle the complex effect of phytoplankton-microbe interactions on marine nitrogen biogeochemistry.

Plain Language Summary Nitrite is a key intermediate between reduced and oxidized forms of nitrogen that is involved in numerous biological processes in the marine nitrogen cycle. Throughout the world's oceans, concentrations of nitrite vary spatially, with concentrations in the subtropics often demonstrating a subsurface maximum, while concentrations are often elevated in the euphotic zone in the tropics and subpolar regions. To date, the mechanisms and processes governing the vertical distributions of nitrite remain controversial. By investigating a suite of processes catalyzing nitrite cycling across the Northwestern Pacific, we show that spatially variable interactions between phytoplankton and planktonic nitrifiers regulate pathways and rates of nitrite cycling. These processes together shape nitrite distribution patterns at the basin scale. Additionally, we demonstrate the significance of urea oxidation in marine nitrogen recycling in terms of contributing to the primary nitrite maximum formation and maintaining the homeostasis of the two steps of nitrification.

1. Introduction

Nitrogen (N) limits primary productivity in approximately half of the global ocean, with concomitant influences on the magnitude of ocean carbon sequestration (Falkowski, 1997; Moore et al., 2013). Despite the importance of N cycling in global biogeochemistry, our knowledge of the complicated and interactive microbially-mediated transformations among N species remains incomplete. The marine N cycle is structured by a series of redox-driven biological transformations between the major N species, from the most reduced forms of ammonium (NH_4^+) and organic N to the most oxidized form nitrate (NO_3^-). As an intermediate in many of these processes, nitrite (NO_2^-) plays numerous roles in plankton metabolism, including acting

Visualization: Xianhui S. Wan, Hua-Xia Sheng, Matthew J. Church, Bess B. Ward
Writing – original draft: Xianhui S. Wan, Hua-Xia Sheng
Writing – review & editing: Xianhui S. Wan, Hua-Xia Sheng, Minhan Dai, Matthew J. Church, Wenbin Zou, Xiaolin Li, David A. Hutchins, Bess B. Ward

as an electron donor or acceptor for diverse microorganisms, a nutrient source for phytoplankton (NO_2^- assimilation), and a metabolic product of ammonia-oxidizing organisms (AOO). Hence, NO_2^- is centrally involved in multiple processes that structure the marine N cycle, making it an excellent intermediate for disentangling marine N biogeochemistry (Casciotti, 2016).

In well-oxygenated ocean waters, NO_2^- is typically found at very low concentrations (i.e., usually <10 nmol L^{-1}) (Dore & Karl, 1996a; Zafiriou et al., 1992). However, in stratified regions of the world's oceans NO_2^- can accumulate (typically 100 to 1,000 nmol L^{-1}) near the base of the euphotic zone, forming a vertically unimodal feature known as the primary NO_2^- maximum (PNM; Gruber, 2008; Karl et al., 2008; Lomas & Lipschultz, 2006; Vaccaro & Ryther, 1960). Recent measurements of NO_2^- concentrations in the global ocean show distinct geographic NO_2^- distribution patterns, with the PNM layer vertically ascending from near the base of the euphotic zone in the subtropics into the well-lit, near-surface ocean in the subpolar regions (Cavagna et al., 2015; Kemeny et al., 2016; Olsen et al., 2016; Peng et al., 2018). Mechanisms for the formation and maintenance of this unique global NO_2^- accumulation pattern have recently been modeled as governed by competition with phytoplankton for N sources (Zakem et al., 2018). In this model, competitive interactions between nitrifiers and phytoplankton were controlled by factors such as nitrogen, light, or iron, with nitrifiers outcompeted by faster-growing phytoplankton in N-limiting environments, while these organisms coexist under conditions where phytoplankton growth is limited by light or iron (Zakem et al., 2018). However, field-based quantifications of specific contributions by phytoplankton and nitrifiers as sources and sinks of NO_2^- in the euphotic zone remain limited.

In the sunlit ocean, the release of NO_2^- by marine phytoplankton during incomplete assimilatory reduction of NO_3^- and NH_4^+ oxidation by AOO are considered the dominant NO_2^- sources, but the relative importance and environmental control of these NO_2^- sources are still debated (Casciotti, 2016; Karl & Michaels, 2018; Lomas & Lipschultz, 2006). Several recent studies highlight that urea, an intracellular metabolic byproduct, can act as an alternative substrate fueling the energetic demands of marine AOO (Alonso-Sáez et al., 2012; Bayer et al., 2016; Kitzinger et al., 2019), suggesting a previously unaccounted source of NO_2^- whose contribution to the PNM remains unquantified. Primary sinks for NO_2^- in the oxygenated ocean include NO_2^- oxidation by NO_2^- oxidizing bacteria (NOB), NO_2^- assimilation by phytoplankton and bacteria, and NO_2^- reduction to N_2 in low oxygen microenvironments (Bianchi et al., 2018; Klawonn et al., 2015; Stocker, 2012). To date, the assessment of factors regulating NO_2^- turnover in the upper water column is hindered by limited simultaneous rate measurements of production and consumption processes.

Light has been long recognized as a key factor in forming and maintaining the PNM, either for its regulation of incomplete NO_3^- assimilation (Kiefer et al., 1976; Vaccaro & Ryther, 1960; Wada & Hattori, 1971) or its inhibition of the two steps of nitrification (Dore & Karl, 1996b; Guerrero & Jones, 1996a, 1996b; Olson, 1981; Ward et al., 1982). Surprisingly, the effects of light on NO_2^- production and consumption, including how diel variation in light might regulate NO_2^- distributions, are poorly studied. Moreover, rates of nitrification appear spatially and temporally variable in the near-surface waters of the ocean, suggesting light cannot be the sole factor controlling rates of nitrification in the upper ocean (Shiozaki et al., 2016; Ward, 2008; Yool et al., 2007). In addition to a possible control by light, ambient NO_3^- has also been shown to be a key factor co-regulating competition between phytoplankton and AOO for NH_4^+, with increased NO_3^- concentrations ameliorating phytoplankton-AOO competition for NH_4^+ (Wan et al., 2018). Such findings further imply ambient NO_3^- conditions may also influence NO_2^- distributions and cycling through phytoplankton-nitrifier interactions, although the potential effect of NO_3^- on NO_2^- competition between phytoplankton and the NOB has not yet been investigated.

We conducted a comprehensive suite of rate measurements involved in NO_2^- production (NH_4^+ oxidation, urea oxidation, and incomplete NO_3^- reduction) and consumption (NO_2^- oxidation, NO_2^- assimilation, and NO_2^- reduction to N_2) across a large region of the open waters of the North Pacific (Figure 1a and Figure S1 in Supporting Information S1). Multiple isotope-labeling incubations were conducted across biogeochemical and physical gradients between the center of the North Pacific Subtropical Gyre (NPSG) and the Subarctic Front (SAF). Rate measurements above, in, and below the PNM were used to identify the NO_2^- cycling processes that determine the distributions and turnover of NO_2^- in these regions. Paired light and dark incubations were used to examine how sunlight influenced NO_2^- metabolism in the upper ocean. The results are expected to elucidate the combined effect of NO_3^- supply and light on NO_2^- cycling; to quantify the

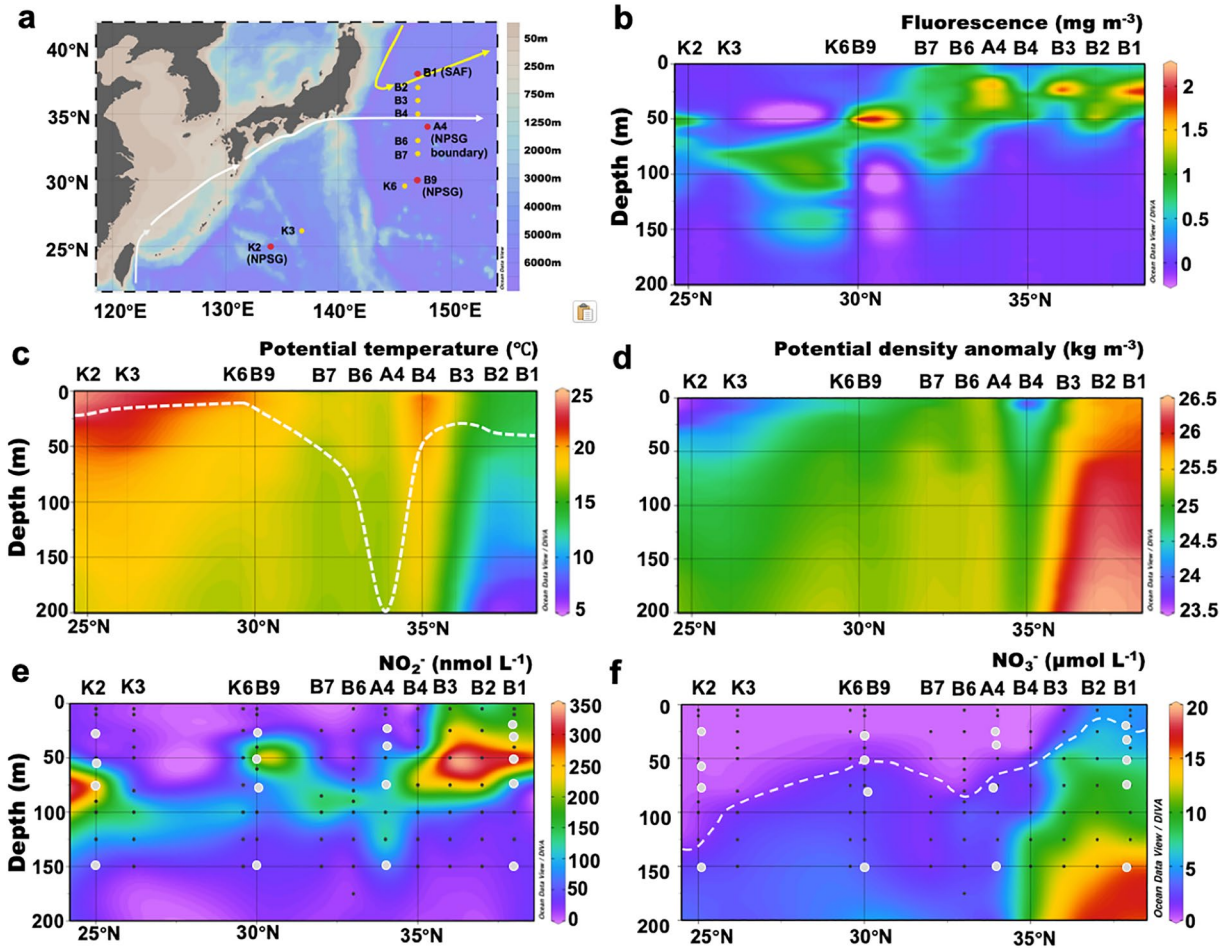

Figure 1. Hydrographic conditions and nutrient distributions along the sampling transect. (a) Research area and sampling stations. Red dots show stations where incubations were conducted, yellow dots depict stations where nutrients were sampled. The white line denotes the boundary of the NPSG and the yellow line shows the boundary of the SAF. (b)–(d) Fluorescence, potential temperature and potential density anomaly of the upper 200 m along the transect. (e)–(f) Distributions of NO_2^- and NO_3^- concentrations in the upper 200 m along the transect. The dashed line in panel c indicates the depth of the upper mixed layer; the dashed line in panel f depict 1 μmol N L^{-1} NO_3^-. The gray dots in panel e and f show the location for on-board incubation. The *x*-axis shows the latitude of each sampling station.

contribution of urea oxidation on PNM formation; and finally, to improve our mechanistic understanding of the processes that shape the enigmatic distribution of this key intermediate in the marine N cycle.

2. Materials and Methods

2.1. Sample Collection and On-Deck Incubations

Sampling for this study was conducted during April–May 2015 aboard the R/V *Dongfanghong II*. Shipboard sampling occurred as part of a transect that extended from the center of the NPSG to the SAF. Four stations (K2, B9, A4, and B1) that spanned large productivity gradients were selected for NO_2^--focused rate measurements (inferred from the surface Chl-a, Figure S2 in Supporting Information S1). Seawater samples were collected using 24 × 12-L Niskin bottles mounted to a CTD rosette equipped with a Seabird SBE 911 CTD sensor package (for measurements of temperature, conductivity, and pressure). In addition, a SeaTech flash fluorometer and a photosynthetically active radiation (PAR) sensor (Li-Cor Biosciences, LI-193) were deployed on the rosette for associated fluorescence and downwelling PAR measurements. Measurements of hydrographic variability and light penetration were obtained by CTD hydrocasts conducted at approximately noon the day prior to rate measurement sampling at the same station.

Samples for subsequent nutrient determinations and rate measurements were collected from CTD hydrocasts conducted at dawn (05:00 to 06:00 local time) for each station. Three 125 mL acid-washed, seawater rinsed, high-density polyethylene (HDPE) bottles were used for nutrient collection; samples for subsequent analysis of urea concentrations were collected into acid-washed, precombusted (450°C for 4 h) 50 mL amber glass vials. Samples for subsequent determinations of particulate nitrogen (PN) concentrations were subsampled from the CTD rosette bottles into acid-washed, seawater rinsed 1 L polycarbonate (PC) bottles.

Samples for rates of NO_2^- reduction to N_2 were subsampled into acid-washed, precombusted (450 °C for 4 h) 120 mL borosilicate serum bottles (CNW, Germany) using Tygon tubing directly from the Niskin bottles. Each sampling bottle was filled to the top and overfilled two to three volumes to minimize the introduction of bubbles. The bottle was then sealed with 20 mm butyl stopper and aluminum seals (Wheaton, USA), followed by removal of 1 mL of a sample using a syringe to allow tracer and $HgCl_2$ injections. Seawater for rate measurements of NH_4^+, urea, NO_2^- oxidation, and NO_3^- reduction were subsampled into 250 mL PC bottles. Samples for NO_2^- uptake incubations were subsampled from the CTD rosette bottles into acid-washed, seawater rinsed 1 L PC bottles. All incubations were carried out in triplicate for each treatment.

Samples for NH_4^+, urea, and NO_2^- oxidation, NO_3^- reduction, and NO_2^- uptake were incubated on-deck under paired light and dark conditions. Four to five depths spanning large light and NO_3^- gradients at each site were selected for on-deck incubations. For light incubations, neutral density screens (Lee Filters) were used to simulate the near *in situ* light intensity; bottles were incubated in an on-deck, surface seawater circulating system. Daily integrated PAR flux was computed from 1 min interval measurements of incident light using a deckboard PAR sensor during the period of incubations. For dark incubations, bottles were wrapped with aluminum foil and placed in dark plastic bags to avoid light contamination. Light and dark incubations were conducted in parallel to examine the potential influences of light on rates and for the subsequent derivation of daily rate estimates. For NO_2^- reduction to N_2, only dark incubations were conducted.

For NH_4^+ and urea oxidation rates, 30 nmol N L^{-1} (final concentration) of ^{15}N-NH_4^+ or ^{15}N-urea (98% of ^{15}N atom, Sigma-Aldrich) and 0.5 μmol N L^{-1} (final concentration) of ^{14}N-NO_2^- carrier were added to each 250-mL incubation bottle containing seawater. For NO_2^- oxidation rates, 30 nmol N L^{-1} (final concentration) of ^{15}N- NO_2^- (98% of ^{15}N atom, Sigma-Aldrich) was added to incubation bottles. For rates of NO_3^- reduction to NO_2^-, seawater incubation bottles were amended with either 30 nmol N L^{-1} (mixed layer samples) or 200 nmol N L^{-1} (for depths deeper than the mixed layer) ^{15}N-NO_3^- (98% of 15N atom, Sigma-Aldrich), and 0.5 μmol N L^{-1} of ^{14}N- NO_2^- carrier. For NO_2^- uptake rates, 30 nmol N L^{-1} (final concentration) of ^{15}N-NO_2^- tracer (98% of ^{15}N atom, Sigma-Aldrich) was added to each bottle. For NO_2^- reduction to N_2, 0.2 mL of ^{15}N-NO_2^- (98% of ^{15}N atom, Sigma-Aldrich) was injected into each bottle for a final tracer concentration of 300 nmol N L^{-1}.

For NH_4^+, urea, and NO_2^- oxidation and NO_3^- reduction measurements, approximately 40 mL of seawater was filtered through a 0.2-μm syringe filter immediately after the addition of ^{15}N tracers; these samples served as time zero controls. The remaining water was incubated under simulated near *in situ* light and dark conditions for 12 h (07:00 -19:00). Incubations were terminated by syringe filtering 40 mL of water through the 25-mm diameter, 0.2-μm polyethersulfone filters. For NO_2^- uptake, triplicate bottles were filtered (with a pressure of ~200 mm Hg) onto pre-combusted (450°C, 4 h) 25-mm glass fiber filters (GF/F, Whatman) immediately after the addition of ^{15}N tracers to represent the initial conditions. The remaining bottles were incubated for 3 h (07:00 - 10:00) on board under simulated near *in situ* light and dark conditions, with incubations terminated by gentle filtration. For NO_2^- reduction to N_2, immediately after $^{15}NO_2^-$ tracer injection triplicate bottles were preserved with 0.1 mL saturated $HgCl_2$, and the remaining bottles incubated in the dark for 24–48 h. Incubations were terminated by the addition of 0.1 mL saturated $HgCl_2$. Samples for subsequent N_2 determinations were stored at 4°C, while all other seawater and membrane samples were stored at −20°C.

2.2. Chemical Measurements

NH_4^+ concentrations were measured aboard the research vessel immediately after collection using a fluorometric method (Zhu et al., 2013) with a detection limit of 1.2 nmol N L^{-1} and a precision of ±3.5%. Seawater samples for quantifying concentrations of other nutrients were stored at −20°C until measurements in the

shore-based lab. Urea concentrations were measured using a 1 m length liquid waveguide capillary cell based on the colorimetric reaction with diacetyl monoxime with a detection limit of 1 nmol N L^{-1} (Chen et al., 2015). NO_2^- and NO_3^- below the nitracline were measured using a four-channel Continuous Flow Technicon AA3 Auto-Analyzer (Bran-Lube, GmbH), with detection limits of 40 nmol N L^{-1} and 70 nmol N L^{-1}, respectively, and precision better than 1% (Wan et al., 2018). Samples with concentrations of NO_3^- and NO_2^- that were near or below the detection limit of the AA3 were analyzed using standard colorimetric methods coupled to a Flow Injection Analysis-Liquid Waveguide Capillary Cell system (World Precision Instruments; Zhang, 2000), with a lower detection limit of 5 nmol N L^{-1} and precision of better than 3%. PN concentrations were determined based on the oxidation of sample filters using purified persulfate as an oxidizing reagent (Knapp et al., 2005), with NO_3^- concentrations subsequently measured by chemiluminescence (Braman & Hendrix, 1989) with a precision of ±5% at the range of measured PN concentrations.

2.3. Isotopic Analyses

$\delta^{15}N$ of NO_2^- was measured by chemical conversion (sodium azide, Sigma-Aldrich) of NO_2^- to N_2O (Mcllvin & Altabet, 2005). To determine NO_2^- oxidation rates, the NO_2^- was initially removed from samples by adding sulfamic acid (≥99% sulfamic acid, Sigma-Aldrich) (Granger & Sigman, 2009) and the $\delta^{15}N$ of NO_3^- was determined using the bacterial denitrifier method (Casciotti et al., 2002; Sigman et al., 2001) with minor modifications. Briefly, NO_3^- was quantitatively converted to N_2O using the bacterial strain *Pseudomonas aureofaciens* (ATCC No. 13985), and N_2O was quantified using a Thermo Finnigan Gasbench system (including cryogenic extraction and purification) interfaced to a Delta V^{PLUS} isotopic ratio mass spectrometer. $\delta^{15}N$ of NO_2^- values were calibrated against three in-house NO_2^- standards ($\delta^{15}N$ of the three in-house NO_2^- standards were determined using the bacterial method, with values of 0.52 ± 0.35‰, 22.06 ± 0.46‰ and 96.27 ± 0.57‰, respectively). Standard curves were run at the beginning and end of sample analysis and at 10 sample intervals. Accuracy (pooled standard deviation) based on analyses of standards at 10 nmol N was ±0.4‰. $\delta^{15}N$ of NO_3^- values were calibrated against NO_3^- isotope standards USGS 34, IAEA N3, and USGS 32, which were run before, after, and at 10 sample intervals. Accuracy (pooled standard deviation) was better than ± 0.2‰ according to analyses of these standards at an injection level of 20 nmol N. Quality control was also conducted by analyzing laboratory working reference material (3,000 m deep sea water from the South China Sea). For samples with NO_3^- concentrations lower than 0.5 μmol N L^{-1}, 1 mL of 5 μmol N L^{-1} of in-house NO_3^- standard was added as a carrier to 9 mL of sample seawater, and the isotopic composition of the sample was then calculated from the measured composition of the mixture and the known in-house standard via mass conservation. For $\delta^{15}N\text{-}N_2$ measurement, 5 mL of seawater was transferred into 20-mL helium pre-purged glass vials to avoid air contamination; $\delta^{15}N\text{-}N_2$ was quantified using a Thermo Finnigan Delta V^{plus} IRMS equipped with Gasbench (including cryogenic extraction and dilution system). The precision of $\delta^{15}N\text{-}N_2$ was better than 0.3‰.

The isotopic composition of PN from incubation experiments was determined using the bacterial denitrifier method following persulfate digestion. In brief, the PN filters were placed in 12-mL pre-combusted borosilicate vials with 1 mL of purified persulfate reagent (POR; final concentration of ~200 mmol L^{-1}). The POR (ACS-grade, Merck, German) was recrystallized at least three times prior to use and residual NO_3^- in the initial POR was quantified and ensured to be sufficiently low (<2 μmol N L^{-1} in digested solution). Samples were autoclaved for 1 h at 120°C. At least five tubes containing only the POR were used to quantify the post-digestion $\delta^{15}N$ blanks. Unused, pre-combusted filters were used to quantify N concentrations and $\delta^{15}N$ values associated with filters (i.e., filter blanks). The $\delta^{15}N$ values of the PN-derived NO_3^- were determined using the bacterial method as described above. Calculation of the concentration and $\delta^{15}N$ of the PN included separate corrections for both the blank of the POR procedure and the filters. The PN blank in each tube was typically less than 1% of the total N and the blank of the filter was less than 5 nmol N (3.99 ± 1.49 nmol N), equivalent to <3% of the N content measured in our samples.

2.4. Rate Calibrations

The reaction rates were determined based on the accumulation of ^{15}N in the product pool relative to the initial (time zero) conditions. To minimize the potential enhancement of the *in-situ* rates due to enrichment by tracer concentrations, the final concentrations of $^{15}N\text{-}NH_4^+$, ^{15}N-urea, and $^{15}N\text{-}NO_2^-$ were limited

to 30 nmol L^{-1}; the corresponding mean *in situ* concentrations of these pools was 83 ± 59, 132 ± 38 and 114 ± 103 nmol L^{-1}, with the tracers accounting for 36 ± 26%, 23 ± 6%, 26 ± 24% of the *in-situ* substrate concentrations, respectively. The final concentrations of NH_4^+, urea, and NO_2^- in our incubations were close to or lower than the half-saturation constant of the reported NH_4^+ (Wan et al., 2018; Zhang et al., 2020), urea (Xu et al., 2019) and NO_2^- oxidation rates (Sun et al., 2017; Zhang et al., 2020), suggesting an overall substrate limiting condition in our incubations. Therefore, we applied a linear regression approach using Equations 1 and 2, with the following assumptions, to obtain the estimates of the *in-situ* reaction rates (Wan et al., 2018).

$$R_{bulk} = \frac{C_t \times n_t - C_0 n_0}{t \times f^{15}} \quad (1)$$

$$R_{in\text{-}situ} = R_{bulk} \times \frac{Ci_s}{Ci_s + Ct_s} \quad (2)$$

R_{bulk} is the bulk reaction rate for all substrates after tracer enrichment (nmol N L^{-1} h^{-1}); Ct and C_0 is the product concentration at the ending and beginning of the incubation (nmol N L^{-1}); f^{15} is at% ^{15}N of the substrate pool at the beginning of the incubation; n_t and n_0 are the at% ^{15}N of the product pool at the ending and beginning of the incubation (%), respectively; t is the duration of the incubation (h); $R_{in\text{-}situ}$ is the *in-situ* reaction rate calibrated by linear interpolation; and Ci_s and Ct_s are the initial substrate concentration and final tracer concentration, respectively. For NH_4^+, urea, and NO_2^- oxidation, NO_3^- reduction, and NO_2^- uptake, the measured rates from light and dark incubations were converted to the daily rates assuming dark incubations approximated nighttime rates and assuming equal photoperiods, that is, the sum of the dark and light hourly rates multiplied by 12 ($R_{\text{in-situ}}$ of light incubation × 12 + $R_{\text{in-situ}}$ of dark incubation × 12). For N_2 production rates, the daily rates were derived using Equation 1.

We quantified the effect of light on NO_2^- transformations based on Equations 3 and 4. Photoinhibition of NH_4^+ oxidation, urea oxidation, and NO_2^- oxidation rates were computed using Equation 3, and reductions in NO_2^- release and NO_2^- uptake in the dark were computed using Equation 4.

$$Inhibition\% = \frac{\left(R_{dark} - R_{light}\right)}{R_{dark}} \times 100\% \quad (3)$$

$$Reduction\% = \frac{\left(R_{light} - R_{dark}\right)}{R_{light}} \times 100\% \quad (4)$$

R_{dark} and R_{light} denote the in-situ conversion rates derived from Equations 1 and 2 under the paired dark and light incubation under near *in situ* light intensity for each depth, respectively.

2.5. Detection Limits of Rate Measurements

The detection limits depend on the concentration of the product pool and the fraction of the ^{15}N in the substrate pool during the incubation. The accuracy of $\delta^{15}N\text{-}NO_3^-$ and $\delta^{15}N\text{-}NO_2^-$ was better than ±0.2‰ and ±0.4‰, respectively, and we here use three times the standard deviation as a reliable enrichment of ^{15}N in each product pool. Therefore, we calculated detection limits of 0.01–0.04 nmol N L^{-1} d^{-1}, 0.01–0.10 nmol N L^{-1} d^{-1}, 0.01–0.49 nmol N L^{-1} d^{-1}, 0.01–0.21 nmol N L^{-1} d^{-1} and 0.01–0.11 nmol N L^{-1} d^{-1} for NH_4^+ oxidation, urea oxidation, NO_2^- oxidation, NO_3^- reduction and NO_2^- uptake rates, respectively. For N_2 production, the corresponding detection limit was 1.12–3.36 nmol N L^{-1} d^{-1}.

3. Results

3.1. Hydrographic and Nutrient Distributions

Vertical patterns in potential temperature, density, and fluorescence showed strong south-north gradients along the transect from NPSG to the SAF (Figures 1b–1d). Elevated near-surface water temperatures and strong stratification were observed in the NPSG stations (K2-B9), where the upper mixed layer depth (MLD)

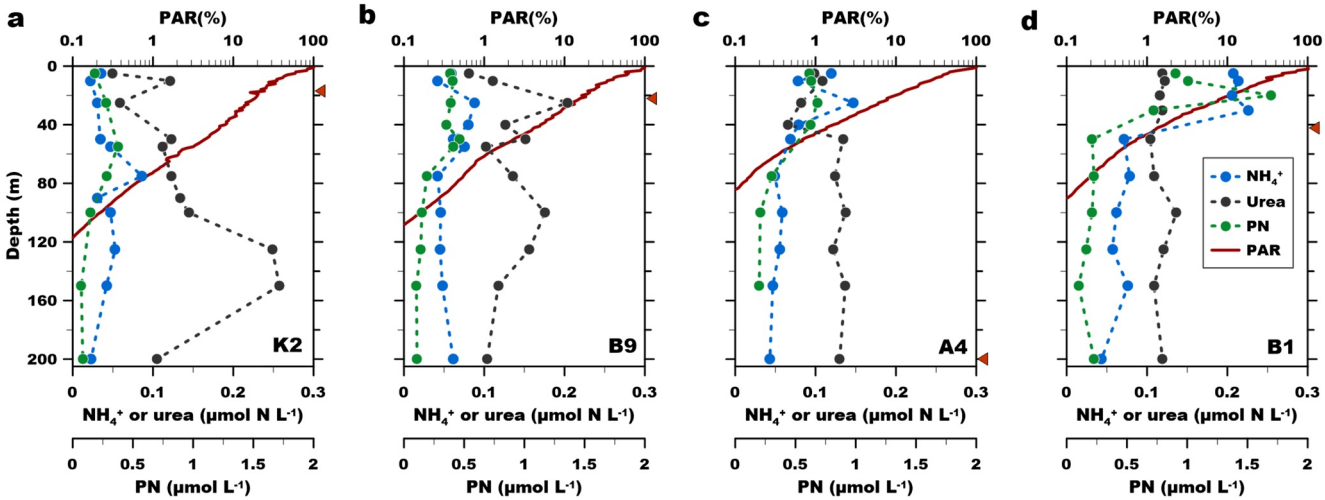

Figure 2. Vertical distributions of NH_4^+, urea, PN concentrations and PAR at the four stations where rate incubations were conducted. (a) Station K2. (b) Station B9. (c) Station A4. (d) Station B1. The red triangle on the right *y*-axis denotes the depth of upper mixed layer.

ranged from 16–25 m based on a temperature threshold criterion with a difference of 0.8°C from the surface value (Kara et al., 2000). By contrast, the upper ocean was well mixed in stations at the boundary of NPSG (stations B6, A4) where the MLD varied from 50-200 m; with stratification weaker along the northern portion of the transect (stations B4 - B1) than in the NPSG. The deep chlorophyll maximum (DCM), as indicated by fluorescence, and the depth of the euphotic zone (defined as 0.1% of surface PAR), shoaled upward toward the north. Daily integrated incident PAR fluxes during the incubation periods were 70.9, 61.3, 43.0, and 69.9 mol m^{-2} d^{-1} at K2, B9, A4, and B1, respectively.

In the subtropical gyre stations (from stations K2 to B6), NO_2^- concentrations displayed the expected PNM structure, with peak concentrations occurring near the base of the euphotic zone. In contrast, at the northern end of the transect (from stations B4 to B1), although NO_2^- concentrations continued to demonstrate subsurface maxima, concentrations were elevated throughout the euphotic zone (Figure 1e). NO_3^- concentrations remained low in the upper mixed layer in the NPSG stations, and the depth of the nitracline (defined as the mid-point (average) of the depth range with the steepest gradient (Aksnes et al., 2007) shoaled upward along the south to north transect, resulting in increased NO_3^- concentrations throughout the euphotic zone in the SAF (Figure 1f).

NH_4^+ concentrations were persistently low at the oligotrophic sites and increased up to ~200 nmol L^{-1} in the well-lit upper ocean at the SAF station B1, although there was no coherent vertical pattern observed at each site (Figure 2; Figure S3 in Supporting Information S1). Upper-ocean concentrations of NH_4^+ tended to increase from south to north, and depth-integrated (0–150 m) NH_4^+ stocks positively correlated with concentrations of PN ($R^2 = 0.96$, $p < 0.05$), suggesting an intensification of remineralization as organic matter stocks increased. Similar to NH_4^+, concentrations of urea demonstrated no consistent vertical patterns, with depth-integrated (0–200 m) stocks of urea 1.3 to 3.7 times larger than NH_4^+ (Table S1 in Supporting Information S1). PN concentrations in the upper 200 m increased into the mid-latitude stations (Figure 2).

3.2. Rates of NO_2^- Conversion in the Light and Dark

3.2.1. NO_2^- Production Rates

The paired light and dark incubations demonstrated light inhibition of ammonia oxidization. The inhibition effect was most prominent in the near-surface waters, decreasing as light attenuated with depth (Figures 3a, 3f, 3k and 3p). Daily NH_4^+ oxidation rates (sum of rates measured in the light and dark) were low to undetectable in the well-lit waters above the nitracline in the oligotrophic stations. In contrast, active NH_4^+ oxidation was observed at the surface layer of the SAF station where concentrations of NO_3^- were elevated. Peak rates of NH_4^+ oxidation were measured in the PNM layer, with rates decreasing with depth below the PNM at all study sites. Urea oxidation rate exhibited a similar vertical distribution pattern to that

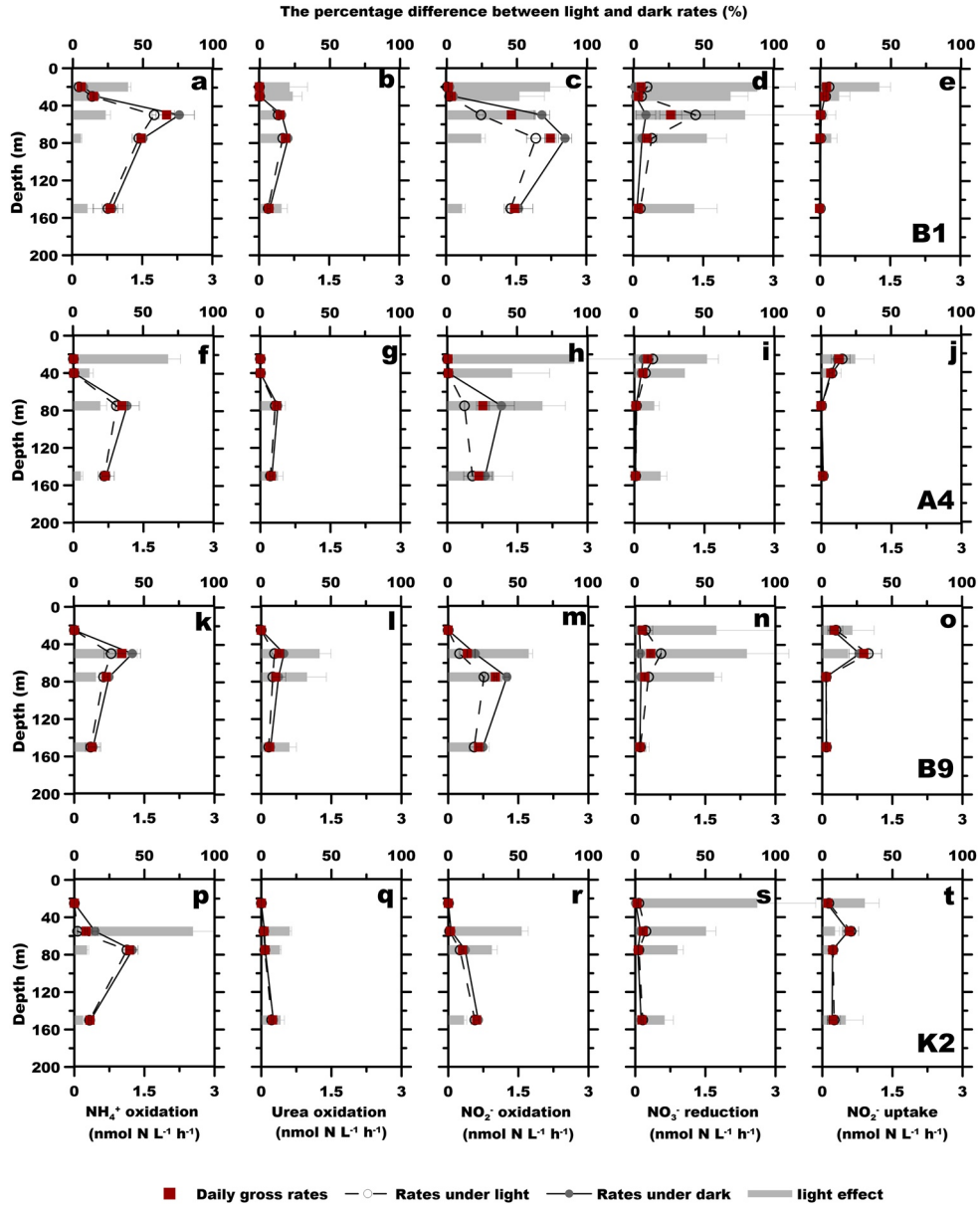

Figure 3. Paired light, dark and daily rates of NO_2^- production and consumption processes. (a)–(e), (f)–(j), (k–o), and (p–t) depict rates measured at stations B1, A4, B9, and K2, respectively. (a, f, k, p) NH_4^+ oxidation rates. (b, g, l, q) urea oxidation rates. (c, h, m, r) NO_2^- oxidation rates. (d, i, h, s) NO_2^- production from NO_3^- reduction and (e, j, o, t) NO_2^- uptake rates. Open and solid gray circles depict rates measured in paired light and dark incubations (nmol N L^{-1} h^{-1}), respectively; red squares are the hourly gross conversion rates (nmol N L^{-1} h^{-1}); gray bars depict the differences between light and dark conversion rates. All error bars depict one standard deviation of triplicate rate measurements; in some cases, the error bars are smaller than the symbols.

of NH_4^+ oxidation in both light and dark conditions (Figures 3b, 3g, 3l and 3q), and the two rates were well correlated ($R^2 = 0.49$, $p < 0.01$). However, urea oxidation rates were 2–50 times lower than NH_4^+ oxidation, despite a much larger inventory of urea (Table S1 in Supporting Information S1).

Rates of NO_3^- reduction to NO_2^- were detectable throughout the euphotic zone (Figures 3d, 3i, 3n and 3s). In contrast to NH_4^+ and urea oxidation processes, the rates of the NO_2^- production via NO_3^- reduction were greatest in the upper euphotic zone, decreasing with depth. Peak NO_2^- production rates from NO_3^- reduction were comparable to the highest rates of urea oxidation but lower than NH_4^+ oxidation; however, the depth of the NO_3^- reduction maximum was sometimes shallower than that of the oxidation rates.

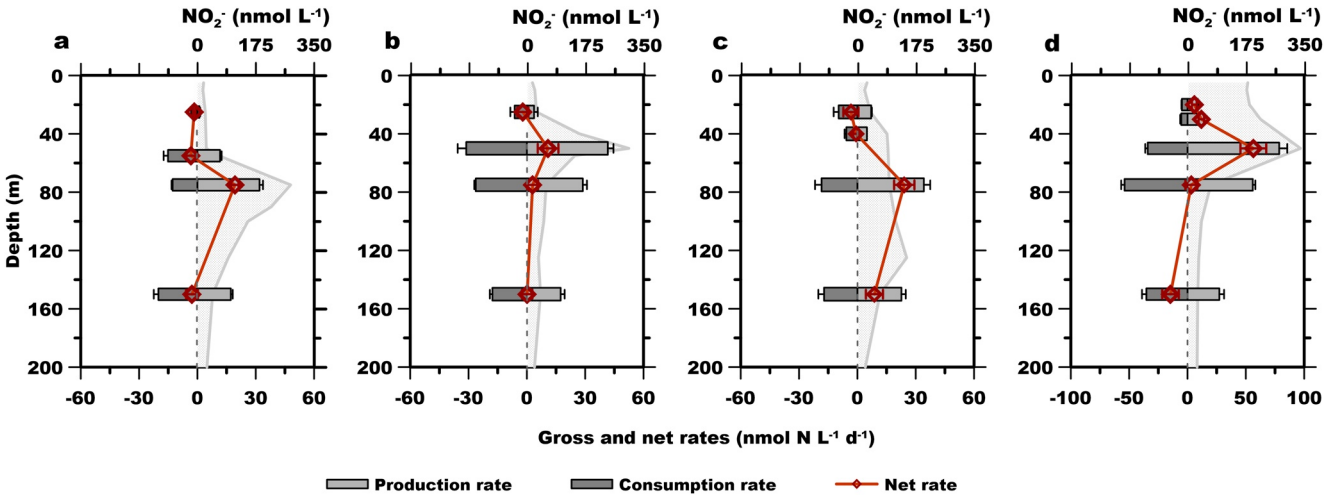

Figure 4. Gross NO_2^- production and consumption rates. (a–d) Rates of the NPSG stations K2, B9, A4 and the high-nitrate SAF station B1, respectively. Horizontal light gray and dark gray bars depict the gross production rates and gross consumption rates (nmol N L^{-1} d^{-1}), respectively; open red diamonds depict the net rates (nmol N L^{-1} d^{-1}), the gray shading depicts distributions of NO_2^- concentrations (nmol N L^{-1}). All error bars are the propagated standard deviation of the rates derived from triplicate incubations. The consumption rates are presented as negative values. Note the scale of *X*-axis for station B1 differs from the remaining stations.

3.3. NO_2^- Consumption Rates

For all of the investigated sites and depths, rates of NO_2^- reduction to N_2 were consistently below the detection limit (<1.1–3.4 nmol N L^{-1} d^{-1} in our incubations), suggesting a negligible role for denitrification and anammox on NO_2^- concentrations and spatial distributions in these well-oxygenated waters.

Similar to rates of NH_4^+ and urea oxidation, rates of NO_2^- oxidation were also influenced by light, with rates depressed at greater light intensities, increasing along the vertical gradient in attenuation (Figures 3c, 3h, 3m and 3r). Light inhibited rates of NO_2^- oxidation to a greater extent than rates of NH_4^+ oxidation, with NO_2^- oxidation rates increasing with depth, peaking below the PNM, before decreasing with increasing depth. The magnitude of the peak NO_2^- oxidation was comparable to the peak NH_4^+ oxidation, but rates of NO_2^- oxidation were often elevated at depths where both NH_4^+ and urea oxidation decreased.

NO_2^- uptake was detectable throughout the euphotic zone with greater rates in the light than in dark (Figures 3e, 3j, 3o and 3t). Peak rates of NO_2^- uptake were observed above the nitracline where the light was replete and NO_3^- concentrations were depleted. Notably, in contrast to rates of other NO_2^- cycling processes, NO_2^- uptake was lowest at station B1 where NO_3^- concentrations were greatest. In profiles where coincident rate measurements were conducted, maximum NO_2^- uptake rates were lower than maximal NO_2^- oxidation (0.1–0.9 fold), suggesting NOB played an important role in consuming NO_2^- in the oxygenated upper ocean.

3.4. Gross and Net NO_2^- Cycling Rates

The suite of rate measurements conducted as part of this study permits us to evaluate coupling among NO_2^- production and consumption rate processes across biogeochemical and physical gradients along the long transect of the North Pacific. The gross NO_2^- production rate (sum of NH_4^+ oxidation, urea oxidation, and NO_3^- reduction to NO_2^-) was low at depths above the nitracline, increasing with depth until reaching a maximum in the PNM layer, and then decreasing at greater depths (Figure 4). The depth of maximal NO_2^- consumption (sum of NO_2^- oxidation, and NO_2^- uptake) varied among stations. Peak rates of NO_2^- consumption occurred in the PNM at station B9, but at greater depths at stations K2 and B1. As a result, the daily integrated rate of NO_2^- production was nearly equivalent to rates of consumption above or below the PNM, with net NO_2^- production consistently observed at depths where NO_2^- concentrations accumulated. Net NO_2^- production rates (the difference between the gross production and gross consumption rate) were spatially correlated with NO_2^- concentrations ($R^2 = 0.69$, $p < 0.01$), while rates of NO_2^- production and

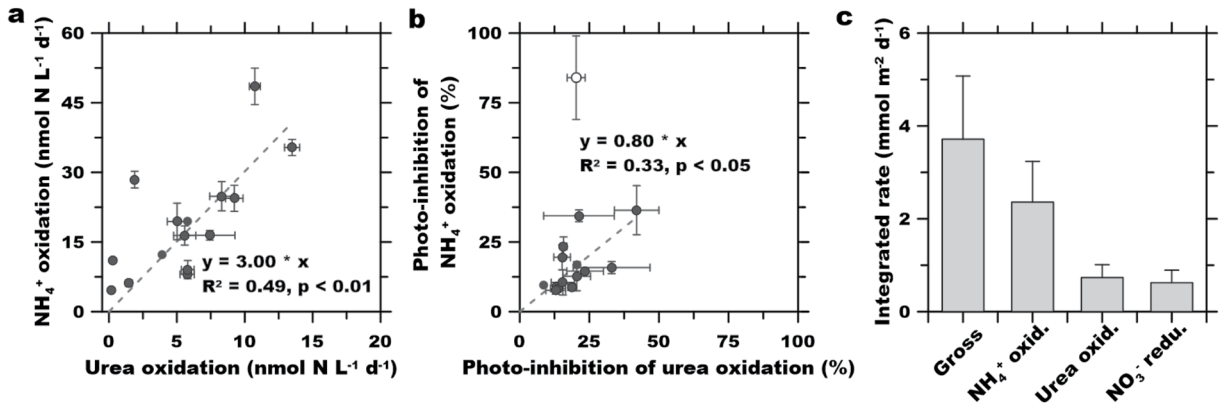

Figure 5. Comparison of NH_4^+ and urea oxidation rates. (a) Least squares linear regression of rates of NH_4^+ oxidation and urea oxidation. (b) Regression of photoinhibition of NH_4^+ oxidation and urea oxidation under paired light-dark incubations; note that one measurement (shown in open dot) was excluded from the regression. (c) Spatially averaged, depth-integrated (0–150 m) rates of gross NO_2^- production (Gross), NH_4^+ oxidation (NH_4^+ oxid.), urea oxidation (urea oxid.), and NO_3^- reduction to NO_2^- (NO_3^- redu.) at study sites.

consumption appeared less significantly correlated with NO_2^- concentrations (Table S1 in Supporting Information S1). These results suggest both production and consumption control NO_2^- distribution and reinforce the necessity of measuring both sources and sinks to understand processes underlying NO_2^- accumulation.

Rates of all the measured processes, except NO_2^- uptake, were greater in the nutrient-replete regions sampled than in the oligotrophic gyres (Figures 3 and 4). Accordingly, both the depth-integrated (0–150 m) production and consumption rates increased from south to north, indicative of simultaneous enhancement of multiple N transformations in the nutrient-replete waters (Table S3 in Supporting Information S1). At station B1 in the SAF region, NO_2^- production (1.8–2.4 times) and consumption (1.7–2.7 times) rates were greater than observed at other sites, with net production rates greatest in the PNM layer.

4. Discussion

4.1. Urea Oxidation is a Significant NO_2^- Source in the Upper Ocean

Urea has been proposed as an alternative substrate for AOO in the marine environment (Alonso-Sáez et al., 2012) and oxidation of urea by AOO has been confirmed in cultures (Bayer et al., 2016; Qin et al., 2014) and detected in coastal waters of the Gulf of Mexico (Kitzinger et al., 2019). Our results revealed that at basin scales across the Pacific Ocean, rates of urea oxidation appear substantial contributors to NO_2^- production. The ratios of rates of NH_4^+ oxidation to urea oxidation were generally restricted to a narrow range (the interquartile range of the ratios was from 2.6 to 4.5), and the two rates were highly correlated (average ratio of 3.0; $R^2 = 0.49$, $p < 0.01$, Figure 5a). Moreover, urea oxidation demonstrated vertical patterns similar to those of NH_4^+ oxidation, and the magnitude of light inhibition on both NH_4^+ and urea oxidation appears similar and co-varied with depth (Figure 5b), consistent with a recent field-based light manipulation experiment (Xu et al., 2019). These findings suggest that urea may be directly utilized by the marine AOO, and that urea oxidation by these microorganisms appears subject to photoinhibition similar to that for NH_4^+ oxidation. Based on a recent assessment of urea decomposition rates measured in the Gulf of Mexico (Kitzinger et al., 2019), we calculate that urea decomposition would contribute only ~0.2% of ^{15}N in the substrate NH_4^+ pool, an amount two orders of magnitude lower than the tracer enrichment used in our parallel ^{15}N-NH_4^+ incubations (with ^{15}N% of NH_4^+ pool of 31.3 ± 10.0%). This low level of ^{15}N-NH_4^+ from ^{15}N-urea decomposition could contribute to a NO_2^- production rate of 0.1 ± 0.1 nmol L^{-1} d^{-1}, which is one to two orders of magnitude lower than the measured ^{15}N-urea oxidation rates. Such results suggested that a large fraction of the measured urea oxidation rate was likely catalyzed by AOO.

In our study, rates of urea oxidation were responsible for as much as 33% of the NO_2^- produced via NH_4^+ oxidation, which is nearly 10 times higher than reported contributions in more eutrophic coastal zones (average of ~3.5% on the coast of Georgia and the Gulf of Mexico) (Damashek et al., 2019; Kitzinger et al., 2019; Tolar et al., 2017). On average, the depth-integrated (0–150 m) urea oxidation rate (0.74 ± 0.28 mmol

m^{-2} d^{-1}) accounted for 20% of gross NO_2^- production (Figure 5c), demonstrating a substantial contribution of urea oxidation to NO_2^- production, findings consistent with recent observations in the Southern California Bight (Laperriere et al., 2021). Additionally, we find NO_2^- oxidation rates exceeded NH_4^+ oxidation rates below the euphotic zone, as was recently reported in the South China Sea (Zhang et al., 2020) and the offshore ETSP (Santoro et al., 2020). The apparent uncoupling between NH_4^+ and NO_2^- oxidation highlights an unaccounted for source of NO_2^- required to maintain the homeostasis between the two steps of nitrification. Including NO_2^- production deriving from urea oxidation may partially explain the observed uncoupling between NO_2^- production and consumption in the dark ocean. Together, these results suggest that urea oxidation is an important and previously overlooked source of NO_2^- for the formation of the PNM and for balancing NO_2^- production and consumption in the oxygenated ocean.

4.2. Impact of Light on NO_2^- Cycling

Paired light-dark incubations confirmed that light was a key determinant on NO_2^- cycling in the sunlit ocean (Dore & Karl, 1996a; Kiefer et al., 1976; Olson, 1981; Vaccaro & Ryther, 1960; Wada & Hattori, 1971; Ward et al., 1982). Specifically, light inhibited rates of NH_4^+, urea, and NO_2^- oxidation, while light stimulated NO_2^- uptake, and NO_2^- production through NO_3^- reduction. Such observations are not unexpected given the role of light in fueling phytoplankton growth (and hence nutrient assimilation) and the known photosensitivities of nitrifying microorganism growth.

While light inhibited both steps of nitrification, the inhibition on NO_2^- oxidizers by light was significantly greater than on NH_4^+ oxidizers ($p = 0.020$) (Figure 3). The integrated daily rates of light and dark of NH_4^+ oxidation exhibited a unimodal structure peaking at the base of the euphotic zone where NO_2^- accumulated. By contrast, peak rates of NO_2^- oxidation occurred below the peak in NH_4^+ oxidation, consistent with stronger light inhibition of NOB than AOO. Moreover, the finding that rates of NO_2^- oxidation tended to be low in the PNM layer is consistent with studies demonstrating low concentrations of the nitrite oxidoreductase enzyme in the euphotic zone of the central Pacific Ocean (Saito et al., 2020). Although the growth of both NOB and AOO are inhibited by light, these organisms demonstrate different photosensitivities (Guerrero & Jones, 1996a, 1996b) that appear both species-specific and wavelength-/dose-dependent (Merbt et al., 2012; Qin et al., 2014). Our results provide additional evidence that rates of NO_2^- oxidation appear to be more sensitive to light than NH_4^+ oxidation, consistent with observations in the central NPSG (Dore & Karl, 1996b; Olson, 1981). Such results highlight that sunlight may be a key factor vertically decoupling the two steps of nitrification in the ocean, with rates of NH_4^+ oxidation greater in the sunlit waters, with relative increases in NO_2^- oxidation rates below the euphotic zone. Moreover, measured rates of NH_4^+ and NO_2^- oxidation were generally greater in incubations conducted in the dark relative to the light, with daily rates peaking near the bottom of the euphotic zone and decreasing with depth, suggesting these rates may be under control by sunlight in the well-lit waters, switching to substrate-supply control in the dimly-lit waters.

Both NO_2^- uptake and NO_2^- release rates by assimilative NO_3^- reduction were greater in the light than in the dark, and the rate difference for NO_2^- release from NO_3^- reduction was higher than for NO_2^- uptake (Figure 3), suggesting intracellular NO_3^- reduction was more dependent on light energy than intracellular NO_2^- reduction. Phytoplankton assimilation of both NO_3^- and NO_2^- are energy-dependent processes, but the assimilative reduction of NO_2^- to NH_4^+ requires more energy than the reduction of NO_3^- to NO_2^- (Lomas & Glibert, 2000; Sciandra & Amara, 1994). Hence, decoupling of these two reductive processes due to excess intracellular NO_3^- reduction could result in accumulation and subsequent release of NO_2^-. This is in line with the higher NO_2^- release rate through assimilatory NO_3^- reduction under light conditions in our incubations and previous lab cultures (Olson et al., 1980; Wada & Hattori, 1971).

In near-surface waters where phytoplankton dominate NO_2^- cycling, gross production and consumption rates in the light incubations exceeded the corresponding rates in the dark incubations by 1.1–2.4-fold, while the rates were slightly lower (0.8 ± 0.2-fold) in the light in the lower euphotic zone (Figure 6). The most significant difference between rates measured in the light and dark was generally observed in the lower euphotic zone where NO_2^- accumulates. In this dimly-lit layer, net NO_2^- production was greater in the light than in the dark, suggesting NO_2^- production by this process might result in daytime accumulation of NO_2^-.

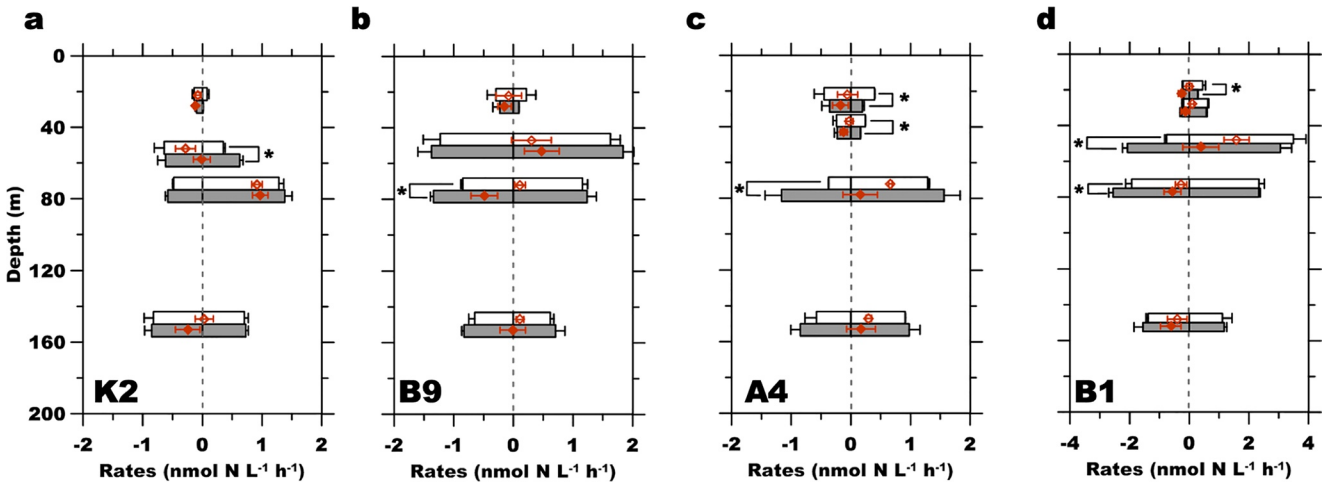

Figure 6. Gross NO_2^- production and consumption rates under paired light and dark incubations. (a–d) Rates of NO_2^- production in the oligotrophic stations K2, B9, A4 and at the subpolar station B1, respectively. The white bars depict gross production rates and gross consumption rates in the light, while dark gray bars show the corresponding gross production rates and gross consumption rates in the dark. The red open and solid diamonds denote net production rates in the light and dark, respectively. All error bars are the propagated standard deviation of the rates derived from triplicate incubations. Note negative value represents consumption. Significant differences between light and dark treatments are denoted by asterisks ($p < 0.05$, student t test).

The urea oxidation and NO_2^- oxidation rates decreased exponentially with the integrated light flux during the incubation periods, while the phytoplankton-associated processes showed weak correlations with light flux, suggesting that light intensity regulated the activities of nitrifiers but was insufficient to explain the phytoplankton mediated rates (Figures S4a–S4e in Supporting Information S1). The difference in rates measured under paired light-dark conditions appeared more tightly correlated with the integrated light flux, suggesting that the light effect on both NO_2^- production and consumption depends on the flux of light experienced by both phytoplankton and nitrifiers in the sunlit ocean, and the NO_2^- oxidation and assimilative NO_3^- reduction processes were more sensitive to light than NH_4^+ oxidation and NO_2^- uptake (Figures S4f–S4j in Supporting Information S1). Together, these results indicate the inclusion of the light effect on NO_2^- cycling via phytoplankton and nitrifiers would be a valuable addition to biogeochemical models simulating the turnover and vertical distributions of NO_2^-. Our findings also point out that seasonal variability in light intensity, daylength, and mixing could be a key factor in determining NO_2^- cycling and PNM distribution. However, the quantitative role of irradiance in NO_2^- dynamics and the potential diel and seasonal variations in NO_2^- cycling remain unexplored in our study and warrants future study.

4.3. Role of Ambient NO_3^- in Determining NO_2^- Cycling and Distributions

In addition to the light effect on NO_2^- producers, and consumers, we suspect other factors may also regulate NO_2^- cycling in the sunlit ocean. For example, rates of NH_4^+ and NO_2^- oxidation were undetectable in the upper euphotic layer in the NPSG, but rates were detectable in the NO_3^--replete SAF despite similar light intensities. In addition, NO_2^- uptake by phytoplankton covaried with NO_2^- release via assimilative NO_3^- reduction in the NPSG, yet the vertical coupling between these processes was not observed in the SAF (Figure 3). Previous studies have shown that phytoplankton has a greater competitive affinity than AOO for NH_4^+ in nutrient-depleted waters (Wan et al., 2018; Zakem et al., 2018). Hence, greater competitive success by phytoplankton for NH_4^+ may depress NH_4^+ oxidation rates in the well-lit surface waters of the oligotrophic NPSG, while in the SAF, where NO_3^- concentrations are elevated in the near-surface waters, competition for NH_4^+ may lessen allowing AOO to maintain appreciable rates of NH_4^+ oxidation. The presence of NO_3^- phytoplankton may reduce nutrient utilization affinity as the mean cell size of communities increases (Irwin et al., 2006; Marañón, 2015). In addition, reduced light exposure due to the deepening of the mixed layer in the SAF would also alleviate the photoinhibition of the AOO (Zakem et al., 2018). A parallel survey of the plankton community and N utilization gene expression in our study area revealed differences in community structure and N utilization strategies with spatial changes in NO_3^- concentrations; this study found NH_4^+ and urea were main sources of N supporting phytoplankton in the NPSG,

while NO_3^- was increasingly more important in the SAF (Li et al., 2018). Indeed, the dominance of NO_3^- as the N source for phytoplankton has been widely observed in nutrient-replete oceans such as the Southern Ocean and the Subarctic North Atlantic (Cavagna et al., 2015; Van Oostende et al., 2017). These results are consistent with NO_3^- concentrations as an important factor regulating NH_4^+ flow through assimilation or oxidation pathways.

To date, few studies have considered potential competition between phytoplankton and NOB for NO_2^- and its impact on NO_2^- distribution. In the nutrient depleted layers of the oligotrophic gyres, phytoplankton biomass is dominated by cyanobacteria, specifically members of *Prochlorococcus* (Campbell et al., 1994; Flombaum et al., 2013; Partensky et al., 1999), including ecotypes capable of utilizing NO_2^- as a potential nitrogen source (Martiny et al., 2009). Our results suggest these cyanobacteria may be superior competitors for NO_2^- relative to NOB in a well-lit oligotrophic ocean. In contrast, phytoplankton and NOB appear to contribute approximately equally to NO_2^- consumption in the near-surface waters of the SAF, suggesting alleviation of NO_2^- competition between NOB and phytoplankton in this region. Moreover, in contrast to other NO_2^- metabolism pathways, NO_2^- uptake rates were significantly lower in the SAF than in the NPSG, suggesting reduced NO_2^- utilization in the more NO_3^- replete waters, potentially reflecting preferential assimilation of NO_3^- rather than NO_2^- by phytoplankton (Mackey et al., 2011; Middelburg & Nieuwenhuize, 2000). Such results could also reflect reduced photoinhibition of NO_2^- oxidation due to deeper mixing in the SAF. Rates of NO_2^- oxidation in the near-surface waters increased along a gradient of increasing NO_3^- concentrations, coincident with decreasing rates of assimilatory NO_2^- uptake (Figure 3), with NOB becoming increasingly dominant in NO_2^- consumption in NO_3^- replete waters. The shoaling of the nitracline thus not only elevated the niche depth of nitrifiers from the subsurface into the well-lit portion of the euphotic zone, but it also supplied NO_3^- to these waters, which may be an important factor controlling microbial NO_2^- metabolism and hence the geographic distribution of NO_2^- in the ocean.

Together, these results underscore a potentially significant and largely overlooked role of NO_3^- in shaping spatial patterns underlying NO_2^- cycling. To further elucidate the potential control of NO_3^- on the NO_2^- distribution in the global surface ocean, we reanalyzed the NO_2^- concentration from the Arctic to the Antarctic ocean in the Western Pacific (Olsen et al., 2016). At the basin scale, the PNM typically occurs near the base of the euphotic zone in the subtropical gyres, shoaling upward in the equatorial and mid-latitudes, resulting in a characteristic 'W'-shaped latitudinal distribution pattern (Figure 7a). Strikingly, the spatial variation of the PNM co-varies with the depth of the 1 μmol L^{-1} NO_3^- (Figure 7b), indicating a tight spatial linkage between NO_3^- supply and NO_2^- accumulation in the sunlit ocean. Moreover, there is a significant correlation between the depth of the NO_2^- maximum and the depth of the nitracline at the basin scale (Figure 7c), suggesting NO_3^- supply may partly influence the geographic distribution of the PNM.

4.4. Distinct NO_2^- Metabolism Processes Above, in, and Below the PNM

We find that in the well-stratified subtropical ocean, phytoplankton dominated both production (35%–100%, average 78 ± 38%) and consumption (93%–100%, average 98 ± 4.2%) of NO_2^- above the PNM (Figure 8). The daily NO_2^- production rate appeared to be slightly lower than the uptake rate, implying that tight coupling of NO_2^- release and re-uptake by phytoplankton prevents the accumulation of NO_2^- in the nutrient limiting environment. Below the nitracline, where light fluxes diminish and NO_3^- concentrations increase, NH_4^+, urea, and NO_2^- oxidation rates increased. Together, these results point to an upper ocean where photoautotrophs regulate NO_2^- cycling, transitioning to NO_2^- cycling catalyzed by chemoautotrophic metabolisms in the dimly-lit deeper waters (Figure 9a). In the dimly-lit and dark waters, NO_2^- oxidation accounted for (31%–92%, averaging 68 ± 25%) of NO_2^- consumption, and NH_4^+ and urea oxidation contributed to (80%–95%, averaging 85 ± 6.0%) of NO_2^- production. However, there was a vertical region where NH_4^+ and NO_2^- oxidation were decoupled, where peak NH_4^+ oxidation was located in the PNM layer with peak NO_2^- oxidation occurring at deeper depths. Thus, we find that the PNM NH_4^+ oxidation, together with urea oxidation and NO_3^- reduction, led to the highest gross rates of NO_2^- production, where NO_2^- production exceeded consumption. Below the PNM layer, where phytoplankton production or consumption of NO_2^- decreased, NO_2^- production decreased with depth, and NO_2^- oxidation rates exceeded NH_4^+ oxidation. Notably, we found that the additional production of NO_2^- through urea oxidation nearly balanced the disparity between NO_2^- oxidation rate and NH_4^+ oxidation rate at these depths. Urea oxidation contributed to 6%–34%,

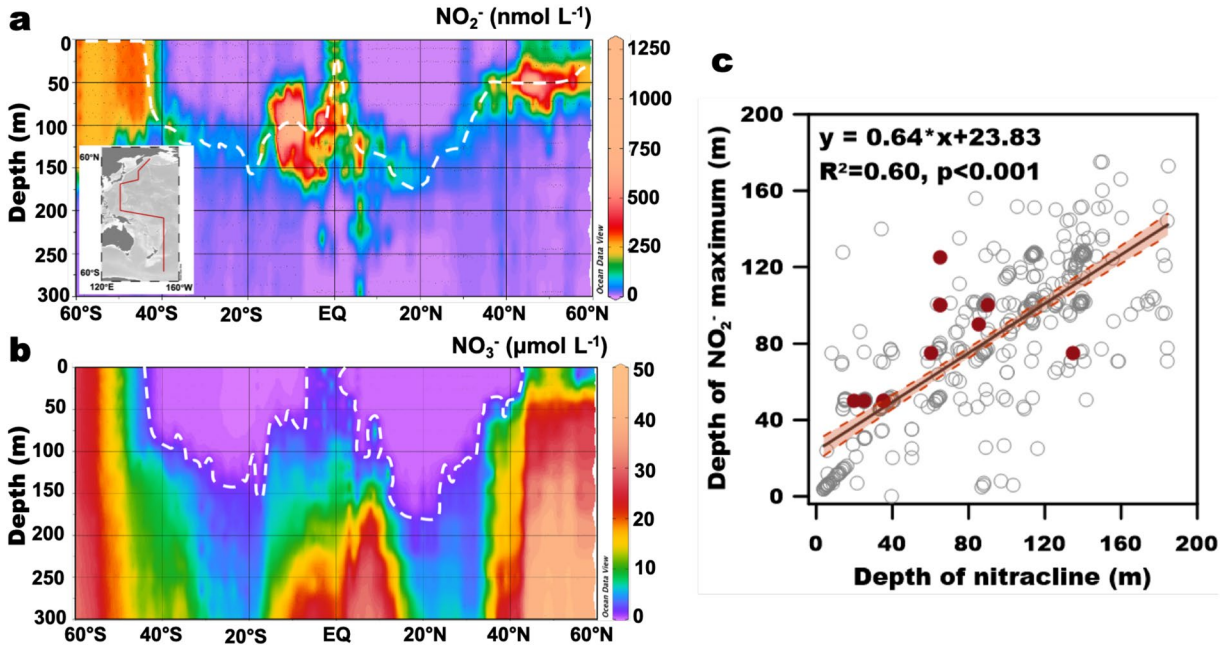

Figure 7. Distribution of NO_2^- and NO_3^- concentrations along a meridional transect in the Pacific. (a–b) Latitudinal NO_2^- and NO_3^- concentrations in the Western Pacific (inserted figure in panel a). The dashed line in panel a indicates the depth of PNM; the dashed lines in panel b indicate the depth where NO_3^- are 1 μmol N L^{-1}; (c) Relationship between the depth of NO_2^- maximum and the depth of nitracline (defined as the mid-point of the depth range with the steepest gradient of NO_3^- except the stations in the sub-Antarctic, where NO_3^- in the upper water column was homogenous, for these stations, the nitracline was set as the shallowest depth sampled during the cruise). The black line and red shadow show linear regressions and the 95% confidence intervals, respectively. The open dots are results from GLODAPv2 database (Olsen et al., 2016); the red circles are results from this study.

(average 24 ± 11%) of NO_2^- production, resulting in near equilibria between rates of NO_2^- production, and consumption below the PNM.

In the SAF region, elevated concentrations of NO_3^- together with deeper mixing (which would decrease light availability) appear to have alleviated competition for both NH_4^+ and NO_2^- between phytoplankton and nitrifiers (Figure 9b). Hence in this region, both photoautotrophic and chemoautotrophic metabolisms contributed to the production and consumption of NO_2^- in the upper euphotic zone. The contribution of NH_4^+ oxidation (averaging 53%) was slightly higher than NO_3^- reduction (averaging 45%) in the upper euphotic zone at B1, reinforcing the role of AOO in providing NO_2^- in these more NO_3^- enriched waters.

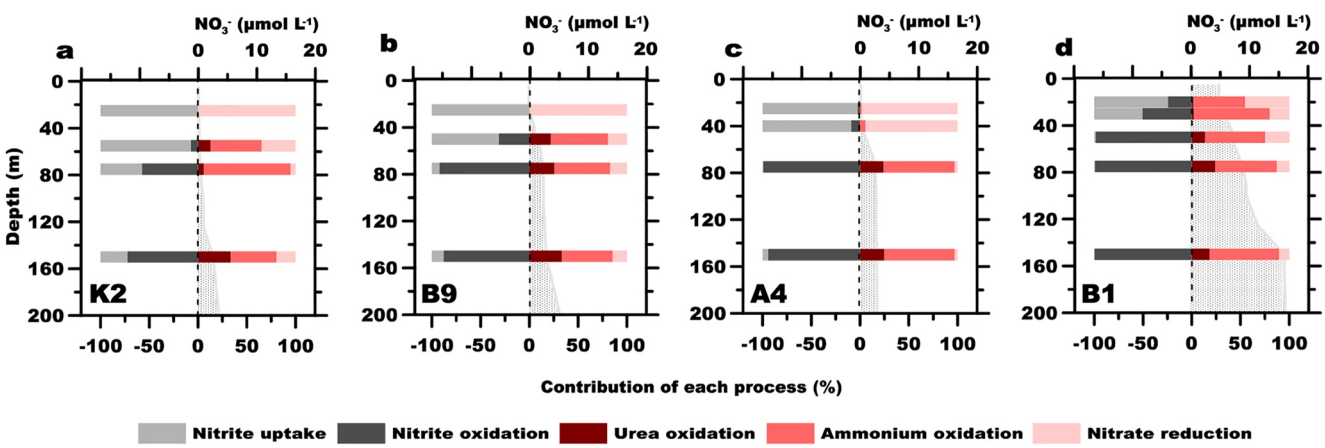

Figure 8. Fractional contribution of NO_2^- cycling processes on the rate of gross production or consumption. (a–d) NPSG stations K2, B9, A4, and the SAF station B1, respectively. The gray shading represents distribution of NO_3^-. Error bars represent propagated standard deviations of the mean rates. Consumption depicted as negative rates.

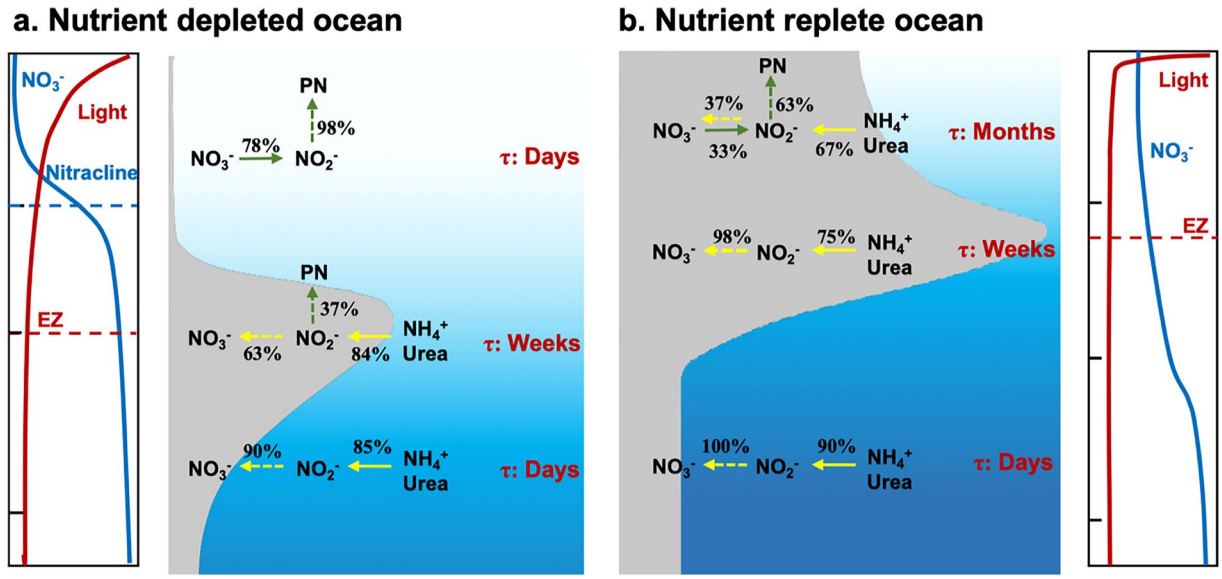

Figure 9. Schematic of the main NO_2^- cycling pathways, turnover and distribution in NO_3^- depleted (a) and NO_3^- enriched ocean (b). Mechanisms controlling the accumulation and turnover of NO_2^- in the nutrient-replete surface ocean appear to differ from those processes controlling NO_2^- cycling at the base of the euphotic zone. τ denotes the scale of NO_2^- residence time. The green and yellow arrows show phytoplankton- and nitrifier-mediated NO_2^- pathways, and the solid and dashed arrows denote production and consumption, respectively. The numbers show the fractional contribution of the main processes (i.e., >30%) to NO_2^- cycling at each depth. Gray shading denotes the NO_2^- concentration profiles.

Moreover, rates of NH_4^+ oxidation were also greater than NO_2^- oxidation rates in the upper ocean in the SAF, with urea oxidation and assimilatory NO_3^- reduction also producing NO_2^-, but NO_2^- uptake was reduced under the elevated NO_3^- concentrations. Thus, we suspect uncoupling between AOO and NOB and additional contribution by incomplete phytoplankton reduction of NO_3^- resulted in a net production of NO_2^- in the upper euphotic zone. In the lower euphotic zone, chemoautotrophic metabolisms appeared to dominate NO_2^- production and consumption, possibly due to the alleviation of light stress. In the PNM layer, vertical decoupling of NH_4^+ oxidation and NO_2^- oxidation appears to permit the accumulation of NO_2^-, while NO_2^- production was nearly equal to or slightly lower than the consumption rate below the PNM, thus maintaining the low concentration of NO_2^-.

The residence time of NO_2^- can be estimated from the concentration divided by either the gross NO_2^- production or consumption rate (Table 1). At the subtropical stations sampled as part of this study, the

Table 1
Residence Time of NO_2^- Above, in and Below the Primary Nitrite Maximum at Study Stations

Station	Depth	Turnover by production (d)	Main production process	Turnover by consumption (d)	Main consumption process
K2	Above PNM	6.4 ± 0.9	NO_3^- reduction	4.8 ± 0.6	NO_2^- uptake
	PNM	8.7 ± 0.5	NH_4^+ oxidation	21.9 ± 1.0	NO_2^- oxidation
	Below PNM	2.6 ± 0.2	NH_4^+ oxidation	2.2 ± 0.3	NO_2^- oxidation
B9	Above PNM	4.3 ± 2.2	NO_3^- reduction	2.6 ± 0.9	NO_2^- uptake
	PNM	7.3 ± 0.6	NH_4^+ oxidation	9.7 ± 1.4	NO_2^- oxidation
	Below PNM	2.1 ± 0.1	NH_4^+ oxidation	2.1 ± 0.0	NO_2^- oxidation
A4[a]	Above DCM	11.3 ± 6.2	NO_3^- reduction	9.4 ± 5.7	NO_2^- uptake
	PNM missing	2.8 ± 0.1	NH_4^+ oxidation	4.4 ± 0.6	NO_2^- oxidation
	Below DCM				
B1	Above PNM	18.0 ± 2.7	NH_4^+ oxidation	39.4 ± 1.1	NO_2^-uptake
	PNM	4.3 ± 0.4	NH_4^+ oxidation	9.9 ± 0.6	NO_2^- oxidation
	Below PNM	0.8 ± 0.2	NH_4^+ oxidation	0.9 ± 0.3	NO_2^- oxidation

[a]No typical PNM structure was observed at the A4 station.

residence time of NO_2^- in the PNM was on the order of weeks (7–22 days for K2 and B9), consistent with observations at BATS (Lipschultz et al., 1996) and ALOHA (Dore & Karl, 1996b) in the oligotrophic Atlantic and Pacific, respectively. Moreover, the residence time of NO_2^- at our oligotrophic stations was greatest in the PNM relative to depths above and below this feature, indicative of a relatively slow turnover of NO_2^-. The longest NO_2^- residence time (18–39 days) was observed in the upper euphotic zone at the northernmost station sampled (B1). Light inhibition of nitrifiers and preferential assimilation of NO_3^- over NO_2^- by phytoplankton might synergistically result in the accumulation and slow turnover of NO_2^- at the surface in this more nutrient-enriched region. However, below the PNM, the activity of nitrifiers significantly enhanced the turnover of NO_2^- at all stations, reducing the residence time to 0.8–2.6 days. These results support the previous finding of longer residence times of NO_2^- in the PNM relative to the euphotic zone or deeper waters (Dore & Karl, 1996b; Santoro et al., 2013), and demonstrate the vertically dynamic processes mediating NO_2^- cycling above, in, and below the PNM, under changing light and nutrient conditions.

Interestingly, the apparent residence time of NO_2^- at the PNM was significantly shorter when calculated using the NO_2^- production rate than when using the NO_2^- consumption rate. This suggests a quasi-steady state of NO_2^- in the PNM, and indicates involvement of negative feedbacks on NO_2^- accumulation such as stimulation of NOB activities and enhanced physical dispersion of elevated NO_2^- concentrations in order to maintain the homeostasis of NO_2^- distributions. Nevertheless, evidence of the accumulation of NO_2^- at the prominent PNM at K2, B9, and B1 stations, and the significant correlation between net NO_2^- production rate and NO_2^- concentration ($R^2 = 0.69$, $p < 0.01$) strongly suggested the dominance of a biological role in determining NO_2^- distributions at these stations.

5. Conclusions

Our suite of measurements of standing stocks, production, and consumption pathways of NO_2^- across a wide swath of the North Pacific revealed several important dynamics associated with N biogeochemistry. In particular, light appears key to regulating all the individual NO_2^- production and consumption processes. However, we also found that the location of the PNM was strongly correlated with the depth of the nitracline at the basin scale, suggesting NO_3^- concentrations may also influence NO_2^- cycling through competitive interactions between phytoplankton and nitrifiers.

We suggest that nitrate-dependent phytoplankton-nitrifier interactions shape the distinct sources, sinks, and turnover of NO_2^- in different ocean regions. In the nitrate-depleted surface layer of the oligotrophic ocean, tight coupling between NO_2^- release during assimilatory NO_3^- reduction and NO_2^- re-uptake by phytoplankton appears to drive rapid turnover of NO_2^-. In contrast, in nitrate-enriched regions of the SAF, we suggest that NO_3^- may alleviate competition between phytoplankton and nitrifiers for NH_4^+ and reduce NO_2^- uptake by phytoplankton, leading to slow accumulation of NO_2^-. In the PNM, decoupling between NH_4^+ and NO_2^- oxidation, likely due to the higher light sensitivities of NOB than AOA, appear to result in the net production and accumulation of NO_2^-. Below the PNM, rates of NH_4^+ oxidation were outpaced by NO_2^- oxidation, preventing NO_2^- accumulation.

We also provide evidence that urea oxidation represents a key source of NO_2^- in the upper ocean and appears to play a role in forming the PNM and maintaining the balance of NO_2^- production and consumption in the NH_4^+ limited oceans. Such results highlight the role of urea oxidation in the upper ocean and draw attention to the need for additional studies on this pathway.

Finally, interactive control by light and nutrients on NO_2^- cycling points to the importance of time-variable processes such as mixing-stratification dynamics, plankton blooms, and variable food web processes as potential key controls on NO_2^- cycling and the PNM. Such processes would be expected to vary seasonally, particularly in the high latitude region where variation in light intensity, daylength, mixing and nutrient supply would all potentially impact NO_2^- concentrations and distributions (Westberry et al., 2015). The tightly coupled seasonal food web dynamics in the subpolar North Pacific (Miller et al., 1991) could also directly influence NO_2^- cycling through regulating urea production. Moreover, given the current and ongoing changes in light exposure and nutrient supplies in the surface ocean due to enhanced stratification (Hutchins et al., 2019; Moore et al., 2018), our findings provide new information to inform models necessary to predict N biogeochemistry and its feedbacks on the ocean carbon cycle.

Conflict of Interest

The authors declare no conflicts of interest relevant to this study.

Data Availability Statement

All data needed to evaluate the conclusions in the paper are deposited in the Zenodo database that can be accessed through https://doi.org/10.5281/zenodo.5533453.

Acknowledgments
The authors greatly appreciate the help of W. Zhang and Q. Wu during the research cruise to the Northwest Pacific. We also thank T. Huang for the on-board measurement of NH_4^+, Y. Wu for NO_3^- and NO_2^- measurements, L. Chen for urea measurements, L. Li for providing the CTD data, M. Du for collecting the NO_2^- and NO_3^- concentration from the GLODAPv2 database and H. Shen for providing the sea surface Chl-*a* data. This work was supported by the Major Research plan of the National Natural Science Foundation of China through grants 92058204, the Major Program of the National Natural Science Foundation of China through grants 41890802, the Science Fund for Creative Research Groups of the National Natural Science Foundation of China through grants 41721005, and the National Natural Science Foundation of China for Young Scientist through grants 41906040. M. J. C. acknowledges support from the Simons Foundation (award # 721221).

References

Aksnes, D. L., Ohman, M. D., & Rivière, P. (2007). Optical effect on the nitracline in a coastal upwelling area. *Limnology & Oceanography*, *52*, 1179–1187. https://doi.org/10.4319/lo.2007.52.3.1179

Alonso-Sáez, L., Waller, A. S., Mende, D. R., Bakker, K., Farnelid, H., Yager, P. L., et al. (2012). Role for urea in nitrification by polar marine Archaea. *Proceedings of the National Academy of Sciences*, *109*, 17989–17994. https://doi.org/10.1073/pnas.1201914109

Bayer, B., Vojvoda, J., Offre, P., Alves, R. JE., Elisabeth, N. H., Garcia, J. AL., et al. (2016). Physiological and genomic characterization of two novel marine thaumarchaeal strains indicates niche differentiation. *The ISME Journal*, *10*, 1051–1063. https://doi.org/10.1038/ismej.2015.200

Bianchi, D., Webber, T. S., Kiko, R., & Deutsch, C. (2018). Global niche of marine anaerobic metabolisms expanded by particle microenvironments. *Nature Geoscience*, *11*, 263–268. https://doi.org/10.1038/s41561-018-0081-0

Braman, R. S., & Hendrix, S. A. (1989). Nanogram nitrite and nitrate determination in environmental and biological materials by vanadium (III) reduction with chemiluminescence detection. *Analytical Chemistry*, *61*, 2715–2718. https://doi.org/10.1021/ac00199a007

Campbell, L., Nolla, H. A., & Vaulot, D. (1994). The importance of *Prochlorococcus* to community structure in the central North Pacific Ocean. *Limnology & Oceanography*, *39*, 954–961. https://doi.org/10.4319/lo.1994.39.4.0954

Casciotti, K. L. (2016). Nitrite isotopes as tracers of marine N cycle processes. *Philosophical Transactions of the Royal Society A: Mathematical, Physical & Engineering Sciences*, *374*, 20150295. https://doi.org/10.1098/rsta.2015.0295

Casciotti, K. L., Sigman, D. M., Galanter Hastings, M., Böhlke, J. K., & Hilkert, A. (2002). Measurement of the oxygen isotopic composition of nitrate in seawater and freshwater using the denitrifier method. *Analytical Chemistry*, *74*, 4905–4912. https://doi.org/10.1021/ac020113w

Cavagna, A. J., Fripiat, F., Elskens, M., Mangion, P., Chirurgien, L., Closset, I., et al. (2015). Production regime and associated N cycling in the vicinity of Kerguelen Island, Southern Ocean. *Biogeosciences*, *12*, 6515–6528. https://doi.org/10.5194/bg-12-6515-2015

Chen, L., Ma, J., Huang, Y., Dai, M., & Li, X. (2015). Optimization of a colorimetric method to determine trace urea in seawater. *Limnology and Oceanography: Methods*, *13*, 303–311. https://doi.org/10.1002/lom3.10026

Damashek, J., Tolar, B. B., Liu, Q., Okotie-Oyekan, A. O., Wallsgrove, N. J., Popp, B. N., & Hollibaugh, J. T. (2019). Microbial oxidation of nitrogen supplied as selected organic nitrogen compounds in the South Atlantic Bight. *Limnology & Oceanography*, *64*, 982–995. https://doi.org/10.1002/lno.11089

Dore, J. E., & Karl, D. M. (1996a). Nitrite distributions and dynamics at Station ALOHA. *Deep Sea Research Part II: Topical Studies in Oceanography*, *43*, 385–402. https://doi.org/10.1016/0967-0645(95)00105-0

Dore, J. E., & Karl, D. M. (1996b). Nitrification in the euphotic zone as a source for nitrite, nitrate, and nitrous oxide at Station ALOHA. *Limnology & Oceanography*, *41*, 1619–1628. https://doi.org/10.4319/lo.1996.41.8.1619

Falkowski, P. G. (1997). Evolution of the nitrogen cycle and its influence on the biological sequestration of CO_2 in the ocean. *Nature*, *387*, 272–275. https://doi.org/10.1038/387272a0

Flombaum, P., Gallegos, J. L., Gordilo, R. A., Rincón, J., Zabala, L., Jiao, N., et al. (2013). Present and future global distributions of the marine Cyanobacteria *Prochlorococcus* and *Synechococcus*. *Proceedings of the National Academy of Sciences*, *110*, 9824–9829. https://doi.org/10.1073/pnas.1307701110

Granger, J., & Sigman, D. M. (2009). Removal of nitrite with sulfamic acid for nitrate N and O isotope analysis with the denitrifier method. *Rapid Communications in Mass Spectrometry*, *23*, 3753–3762. https://doi.org/10.1002/rcm.4307

Gruber, N. (2008). The marine nitrogen cycle: Overview and challenges. In D. G. Capone, D. A. Bronk, M. R. Mulholland, & E. J. Carpenter (Eds.), *Nitrogen in the marine environment* (pp. 12–50): Elsevier. https://doi.org/10.1016/B978-0-12-372522-6.00001-3

Guerrero, M. A., & Jones, R. D. (1996a). Photoinhibition of marine nitrifying bacteria. I. Photoinhibition of marine nitrifying bacteria. I. Wavelength-dependent response. *Marine Ecology Progress Series*, *141*, 183–192. https://doi.org/10.3354/meps141183

Guerrero, M. A., & Jones, R. D. (1996b). Photoinhibition of marine nitrifying bacteria. II. Dark recovery after monochromatic or polychromatic irradiation. *Marine Ecology Progress Series*, *141*, 193–198. https://doi.org/10.3354/meps141193

Hutchins, D. A., Jansson, J. K., Remais, J. V., Rich, V. I., Singh, B. K., & Trivedi, P. (2019). Climate change microbiology - Problems and perspectives. *Nature Reviews Microbiology*, *17*, 391–396. https://doi.org/10.1038/s41579-019-0178-5

Irwin, A. J., Finkel, Z. V., Schofield, O. M. E., & Falkowski, P. G. (2006). Scaling-up from nutrient physiology to the size-structure of phytoplankton communities. *Journal of Plankton Research*, *28*, 459–471. https://doi.org/10.1093/plankt/fbi148

Kara, A. B., Rochford, P. A., & Hurlburt, H. E. (2000). An optimal definition for ocean mixed layer depth. *Journal of Geophysical Research: Oceans*, *105*, 16803–16821. https://doi.org/10.1029/2000JC900072

Karl, D. M., Bidigare, R. R., Church, M. J., Dore, J. E., Letelier, R. M., Mahaffey, C., & Zehr, J. P. (2008). The nitrogen cycle in the North Pacific trades biome: An evolving paradigm. In D. G. Capone, D. A. Bronk, M. R. Mulholland, & E. J. Carpenter (Eds.), *Nitrogen in the marine environment* (Edn. 2, pp. 7052–7769). Elsevier. https://doi.org/10.1016/B978-0-12-372522-6.00016-5

Karl, D. M., & Michaels, A. F. (2018). Nitrogen Cycle. In J. K. Cochran, H. J. Bokuniewicz, & L. Y. Patricia (Eds.), *Encyclopedia of ocean Sciences* (Edn. 3, pp. 13–417). Academic Press. https://doi.org/10.1016/B978-0-12-409548-9.11608-2

Kemeny, P. C., Weigand, M. A., Zhang, R., Carter, B. R., Karsh, K. L., Fawcett, S. E. & Sigman, D. M. (2016). Enzyme-level interconversion of nitrate and nitrite in the fall mixed layer of the Antarctic Ocean. *Global Biogeochemical Cycles*, *30*, 1069–1085. https://doi.org/10.1002/2015GB005350

Kiefer, D. A., Olson, R. J., & Holm-Hansen, O. (1976). Another look at the nitrite and chlorophyll maxima in the central North Pacific. *Deep Sea Research*, *12*, 1199–1208. https://doi.org/10.1016/0011-7471(76)90895-0

Kitzinger, K., Padilla, C. C., Marchant, H. K., Hach, P. F., Herbold, C. W., Kidane, A. T., et al. (2019). Cyanate and urea are substrates for nitrification by Thaumarchaeota in the marine environment. *Nature Microbiology*, *4*, 234–243. https://doi.org/10.1038/s41564-018-0316-2
Klawonn, I., Bonaglia, S., Bruchert, V., & Ploug, H. (2015). Aerobic and anaerobic nitrogen transformation processes in N_2-fixing cyanobacterial aggregates. *The ISME Journal*, *9*, 1456–1466. https://doi.org/10.1038/ismej.2014.232
Knapp, A. N., Sigman, D. M., & Lipschultz, F. (2005). N isotopic composition of dissolved organic nitrogen and nitrate at the Bermuda Atlantic Time-series Study site. *Global Biogeochemical Cycles*, *19*, GB1018. https://doi.org/10.1029/2004gb002320
Laperriere, S. M., Morando, M., Capone, D. G., Gunderson, T., Smith, J. M., & Santoro, A. E. (2021). Nitrification and nitrous oxide dynamics in the Southern California Bight. *Limnology & Oceanography*, *66*, 1099–1112. https://doi.org/10.1002/lno.11667
Li, Y. Y., Chen, X. H., Xie, Z. X., Li, D. X., Wu, P. F., Kong, L. F., et al. (2018). Bacterial diversity and nitrogen utilization strategies in the upper layer of the Northwestern Pacific Ocean. *Frontiers in Microbiology*, *9*, 797. https://doi.org/10.3389/fmicb.2018.00797
Lipschultz, F., Zafiriou, O. C., & Ball, L. A. (1996). Seasonal fluctuations of nitrite concentrations in the deep oligotrophic ocean. *Deep Sea Research Part II: Topical Studies in Oceanography*, *43*, 403–419. https://doi.org/10.1016/0967-0645(96)00003-3
Lomas, M. W., & Glibert, P. M. (2000). Comparisons of nitrate uptake, storage and reduction in marine diatoms and flagellates. *Journal of Phycology*, *36*, 903–913. https://doi.org/10.1046/j.1529-8817.2000.99029.x
Lomas, M. W., & Lipschultz, F. (2006). Forming the primary nitrite maximum: Nitrifiers or phytoplankton? *Limnology & Oceanography*, *51*, 2453–2467. https://doi.org/10.4319/lo.2006.51.5.2453
Mackey, K. R. M., Bristow, L., Parks, E. R., Altabet, M. A., Post, A. F., & Paytan, A. (2011). The influence of light on nitrogen cycling and the primary nitrite maximum in a seasonally stratified sea. *Progress in Oceanography*, *91*, 545–560. https://doi.org/10.1016/j.pocean.2011.09.001
Marañón, E. (2015). Cell size as a key determinant of phytoplankton metabolism and community structure. *Annual Review of Marine Science*, *7*, 241–264. https://doi.org/10.1146/annurev-marine-010814-015955
Martiny, A. C., Kathuria, S., & Berube, P. M. (2009). Widespread metabolic potential for nitrite and nitrate assimilation among Prochlorococcus ecotypes. *Proceedings of the National Academy of Sciences*, *106*, 10787–10792. https://doi.org/10.1073/pnas.0902532106
Mcllvin, M. R., & Altabet, M. A. (2005). Chemical conversion of nitrate and nitrite to nitrous oxide for nitrogen and oxygen isotopic analysis in freshwater and seawater. *Analytical Chemistry*, *77*, 5589–5595. https://doi.org/10.1021/ac050528s
Merbt, S. N., Stahl, D. A., Casamayor, E. O., Martí, E., Nicol, G. W., & Prosser, J. I. (2012). Differential photoinhibition of bacterial and archaeal ammonia oxidation. *FEMS Microbiology Letters*, *327*, 41–46. https://doi.org/10.1111/j.1574-6968.2011.02457.x
Middelburg, J. J., & Nieuwenhuize, J. (2000). Nitrogen uptake by heterotrophic bacteria and phytoplankton in the nitrate-rich Thames estuary. *Marine Ecology Progress Series*, *203*, 13–21. https://doi.org/10.3354/meps203013
Miller, C. B., Frost, B. W., Wheeler, P. A., Welschmeyer, N., Powell, T. M., & Powell, T. M. (1991). Ecological dynamics in the subarctic Pacific, a possibly iron-limited ecosystem. *Limnology & Oceanography*, *36*, 1600–1615. https://doi.org/10.4319/lo.1991.36.8.1600
Moore, C. M., Mills, M. M., Arrigo, K. R., Berman-Frank, I., Bopp, L., Boyd, P. W., et al. (2013). Processes and patterns of oceanic nutrient limitation. *Nature Geoscience*, *6*, 701–710. https://doi.org/10.1038/Ngeo1765
Moore, J. K., Fu, W., Primeau, F., Britten, G. L., Lindsay, K., Long, M., et al. (2018). Sustained climate warming drives declining marine biological productivity. *Science*, *359*, 1139–1143. https://doi.org/10.1126/science.aao6379
Olsen, A., Key, R. M., van Heuven, S., Lauvset1, S. K., Velo, A., Lin, X., et al. (2016). The global ocean data analysis project version 2 (GLODAPv2)- an internally consistent data product for the world ocean. *Earth Systerm Science Data*, *8*, 297–323. https://doi.org/10.5194/essd-8-297-2016
Olson, R. J. (1981). Differential photoinhibition of marine nitrifying bacteria: A possible mechanism for the formation of the primary nitrite maximum. *Journal of Marine Research*, *39*, 227–238.
Olson, R. J., Soohoo, J. B., & Kiefer, D. A. (1980). Steady-state growth of the marine diatom *Thalassiosira pseudonana*. *Plant Physiology*, *66*, 383–389. https://doi.org/10.1104/pp.66.3.383
Partensky, F., Hess, W. R., & Vaulot, D. (1999). Prochlorococcus, a marine photosynthetic prokaryote of global significance. *Microbiology and Molecular Biology Reviews*, *63*, 106–127. https://doi.org/10.1128/MMBR.63.1.106-12710.1128/mmbr.63.1.106-127.1999
Peng, X., Fawcett, S. E., van Oostende, N., Wolf, M. J., Marconi, D., Sigman, D. M., & Ward, B. B. (2018). Nitrogen uptake and nitrification in the subarctic North Atlantic Ocean. *Limnology & Oceanography*, *63*, 1462–1487. https://doi.org/10.1002/lno.10784
Qin, W., Amin, S. A., Martens-Habbena, W., Walker, C. B., Urakawa, H., Devol, A. H., et al. (2014). Marine ammonia-oxidizing archaeal isolates display obligate mixotrophy and wide ecotypic variation. *Proceedings of the National Academy of Sciences*, *111*, 12504–12509. https://doi.org/10.1073/pnas.1324115111
Saito, M. A., McIlvin, M. R., Moran, D. M., Santoro, A. E., Dupont, C. L., Rafter, P. A., et al. (2020). Abundant nitrite-oxidizing metalloenzymes in the mesopelagic zone of the tropical Pacific Ocean. *Nature Geoscience*, *13*, 355–362. https://doi.org/10.1038/s41561-020-0565-6
Santoro, A. E., Buchwald, C., Knapp, A. N., Berelson, W. M., Capone, D. G., & Casciotti, K. L. (2020). Nitrification and nitrous oxide production in the offshore waters of the Eastern Tropical South Pacific. *Global Biogeochemical Cycles*, *34*, e2020GB006716. https://doi.org/10.1029/2020GB006716
Santoro, A. E., Sakamoto, C. M., Smith, J. M., Piant, J. N., Gehman, A. L., Worden, A. N., et al. (2013). Measurements of nitrite production in and around the primary nitrite maximum in the central California Current. *Biogeosciences*, *10*, 7395–7410. https://doi.org/10.5194/bg-10-7395-2013
Sciandra, A., & Amara, R. (1994). Effects of nitrogen limitation on growth and nitrite excretion rates of the dinoflagellate *Prorocentrum minimum*. *Marine Ecology Progress Series*, *105*, 301–309. https://doi.org/10.3354/meps105301
Shiozaki, T., Ijichi, M., Isobe, K., Hashihama, F., Nakamura, K. I., Ehama, M., et al. (2016). Nitrification and its influence on biogeochemical cycles from the equatorial Pacific to the Arctic Ocean. *The ISME Journal*, *10*, 2184–2197. https://doi.org/10.1038/ismej.2016.18
Sigman, D. M., Casciotti, K. L., Andreani, M., Barford, C., Galanter, M., & Böhlke, J. K. (2001). A bacterial method for the nitrogen isotopic analysis of nitrate in seawater and freshwater. *Analytical Chemistry*, *73*, 4145–4153. https://doi.org/10.1021/ac010088e
Stocker, R. (2012). Marine microbes see a sea of gradients. *Science*, *338*, 628–633.
Sun, X., Ji, Q., Jayakumar, A., & Ward, B. B. (2017). Dependence of nitrite oxidation on nitrite and oxygen in low-oxygen seawater. *Geophysical Research Lettters*, *44*, 7883–7891. https://doi.org/10.1002/2017GL074355
Tolar, B. B., Wallsgrove, N. J., Popp, B. N., & Hollibaugh, J. T. (2017). Oxidation of urea-derived nitrogen by thaumarchaeota-dominated marine nitrifying communities. *Environmental Microbiology*, *19*, 4838–4850. https://doi.org/10.1111/1462-2920.13457
Vaccaro, R. F., & Ryther, J. H. (1960). Marine phytoplankton and the distribution of nitrite in the sea. *ICES Journal of Marine Science*, *25*, 260–271. https://doi.org/10.1093/icesjms/25.3.260

Van Oostende, N., Fawcett, S. E., Marconi, D., Lueders-Dumont, J., Sabadel, A. J. M., Woodward, E. M. S., et al. (2017). Variation of summer phytoplankton community composition and its relationship to nitrate and regenerated nitrogen assimilation across the North Atlantic Ocean. *Deep Sea Research Part I: Oceanographic Research Papers*, *121*, 79–94. https://doi.org/10.1016/j.dsr.2016.12.012

Wada, E., & Hattori, A. (1971). Nitrite metabolism in the euphotic layer of the central North Pacific ocean. *Limnology & Oceanography*, *16*, 766–772. https://doi.org/10.4319/lo.1971.16.5.0766

Wan, X. S., Sheng, H. X., Dai, M., Zhang, Y., Shi, D., Trull, T. W., et al. (2018). Ambient nitrate switches the ammonium consumption pathway in the euphotic ocean. *Nature Communications*, *9*, 915. https://doi.org/10.1038/s41467-018-03363-0

Ward, B. B. (2008). Nitrification in marine systems. In D. G. Capone, D. A. Bronk, M. R. Mulholland, & E. J. Carpenter (Eds.), *Nitrogen in the marine environment* (Edn. 2, pp. 1992–2261). Elsevier. https://doi.org/10.1016/B978-0-12-372522-6.00005-0

Ward, B. B., Olson, R. J., & Perry, M. J. (1982). Microbial nitrification rates in the primary nitrite maximum off southern California. *Deep-Sea Research*, *29*, 247–255. https://doi.org/10.1016/0198-0149(82)90112-1

Westberry, T. K., Schultz, P., Behrenfeld, M. J., Dunne, J. P., Hiscock, M. R., Maritorena, S., et al. (2015). Annual cycles of phytoplankton biomass in the subarctic Atlantic and Pacific Ocean. *Global Biogeochemical Cycles*, *30*, 175–190. https://doi.org/10.1002/2015GB005276

Xu, M. N., Li, X., Shi, D., Zhang, Y., Dai, M., Huang, T., et al. (2019). Coupled effect of substrate and light on assimilation and oxidation of regenerated nitrogen in the euphotic ocean. *Limnology & Oceanography*, *64*, 1270–1283. https://doi.org/10.1016/0198-0149(82)90112-1

Yool, A., Martin, A. P., Fernández, C., & Clark, D. R. (2007). The significance of nitrification for oceanic new production. *Nature*, *447*, 999–1002. https://doi.org/10.1038/nature05885

Zafiriou, O. C., Ball, L. A., & Hanley, Q. (1992). Trace nitrite in oxic waters. *Deep Sea Research Part A. Oceanographic Research Papers*, *39*, 1329–1347. https://doi.org/10.1016/0198-0149(92)90072-2

Zakem, E. J., Al-Haj, A., Church, M. J., van Dijken, G. L., Dutkiewicz, S., Foster, S. Q., et al. (2018). Ecological control of nitrite in the upper ocean. *Nature Communications*, *9*, 1206. https://doi.org/10.1038/s41467-018-03553-w

Zhang, J. Z. (2000). Shipboard automated determination of trace concentrations of nitrite and nitrate in oligotrophic water by gas-segmented continuous flow analysis with a liquid waveguide capillary flow cell. *Deep Sea Research Part I: Oceanographic Research Papers*, *47*, 1157–1171. https://doi.org/10.1016/S0967-0637(99)00085-0

Zhang, Y., Qin, W., Hou, L., Zakem, E. J., Wan, X., Zhao, Z., et al. (2020). Nitrifier adaptation to low energy flux controls inventory of reduced nitrogen in the dark ocean. *Proceedings of the National Academy of Sciences*, *117*, 4823–4830. https://doi.org/10.1073/pnas.1912367117

Zhu, Y., Yuan, D., Huang, Y., Ma, J., & Feng, S. (2013). A sensitive flow-batch system for on board determination of ultra-trace ammonium in seawater: Method development and shipboard application. *Analytica Chimica Acta*, *794*, 47–54. https://doi.org/10.1016/j.aca.2013.08.009